Ben Barker
MPhil Thesis:

Thermally actuated magnetic systems

Fitzwilliam College
2005-2006
Supervisor: Dr Tim Coombs

This dissertation is submitted for the degree of Master of Philosophy

List of Contents

List of figures

This dissertation is the result of my own work and includes nothing which is the outcome of work done in collaboration except where specifically indicated in the text

Furthermore, this thesis comes in under the set limit of 15000 words

Signed:

Ben Barker

1 Introduction

This project aims to investigate the possibility of using a thermally actuated magnetic device to achieve controllable, compact magnetic fields through the use of a combination of novel materials and well understood superconductors. This combination of a strong, extremely controllable field that can be accessed on a surface, rather than in a solenoid, would have great advantages. Taking the example of the MRI scanner, rather than patients being confined to a narrow, claustrophobic tube, they could merely lie on a table top. Indeed, since the patient no longer needs to be inside the coil, we might even be able to dispense with the table and merely use a handheld "wand" design. The wand would contain the field, and as long as we can track its position relative to the patient accurately enough, we can compensate for the moving field. And because we only need enough power to trigger each pulse, rather than maintain large currents flowing through a solenoid, systems can be designed to be far smaller and more portable. The idea of using heat and the changing magnetic properties of various materials with temperature to manipulate magnetic fields is not a new one – as far back as 1890 Nikola Tesla himself suggested a device for generating electricity making use of the Curie point of a block of soft iron to disturb flux distribution and generate voltages[1]. However, to the best of our knowledge no attempt has been made to combine this with superconductors in the way we propose to create strong magnetic fields.

1.1 Current options for generation of strong magnetic fields

Strong, uniform magnetic fields have a multitude of uses in our society. High profile examples include MRI[2] scanners, used in hospitals worldwide, magnetic bearings, and certain display systems. However, creating these fields is a problem. Permanent magnetic ferrous materials have their maximum field limited by the number of unpaired electrons in the valence shells. Each unpaired electron produces a magnetic moment, and the sum of these moments normalized for volume gives us the maximum theoretically obtainable field (when all spins are aligned together).

In the case of iron we have a bcc structure with 2.2 unpaired electrons per atom[3]
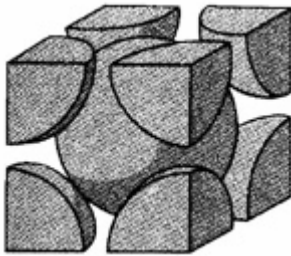
Figure 1-1 – BCC unit cell structure

---

[1]   Nikola Tesla "Pyromagneto-electric generator", US patent office May 1890
[2]   Magnetic Resonance Imaging
[3]   The number of electrons is not a simple integer due to the way the electrons spread out in bcc iron, but the derivation of this value will not be shown here.

The Iron atoms in a BCC unit cell have radii of   ~1.24 Å

If we take a diagonal slice through our BCC cell, we can see that the atoms in the corner each touch the centre atom, giving a diagonal length of 4r, where r is the radius of the Fe atom. We know the unit cell is a cube, thus we can find its sides:

$$L^2 + \left(\sqrt{2}L\right)^2 = (4r)^2$$
$$L^2 + 2L^2 = 16r^2$$
$$3L^2 = 16r^2$$
$$L^2 = \frac{16}{3}r^2$$
$$L = r\sqrt{\frac{16}{3}} = 2.86 \text{ Å}$$
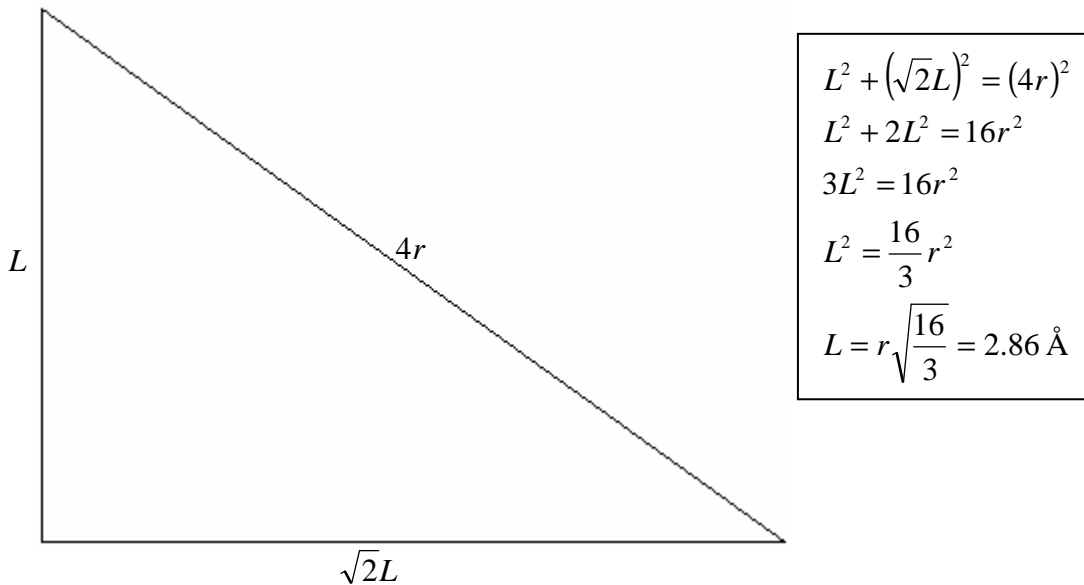
Figure 1-2 – Calculating the size of a unit cell of BCC Fe

The volume is thus L^3, which gives us 23.48 $Å^3$ ($2.34673*10^{-29}\,m^3$)

Each bcc unit cell contains 2 atoms (one central, plus 8 eighths in the corners)
So we have 4.4 unpaired spins per unit cell

The total magnetization is given by the sum of the moments divided by the value
The magnetic moment due to a single electron spin is given by the Bohr magneton,U_b:

U_b=9.27x10^{-24} J/T

$$M = \frac{\sum U_b}{Volume} = (9.27x10^{-24})*4.4 / 2.34673*10^{-29}$$

B=uoM where uo, the permeability of free space, is given by $4\pi \times 10^{-7}$

Thus **B=2.18T**

There are a few elements that have higher saturation magnetizations, but they are not common. In reality the achievable field is lower than the calculated value as not all the spins will align. A realistically achievable figure is of the order of 1.7T.

Permanent magnets also produce non uniform fields. In the example below, flux density is highest at the corners of the material, falling off rapidly towards the centre. Solenoids, where a current is passed through a coil to create a magnetic field, can do better, but at a cost.
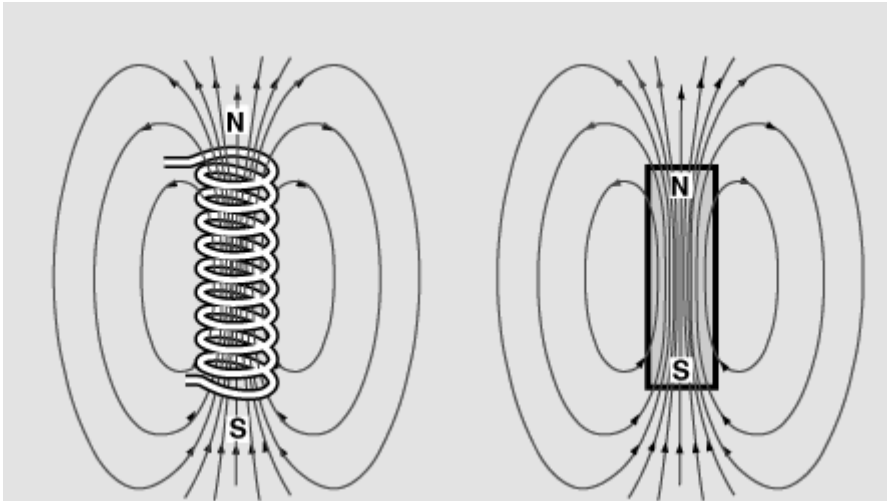
Figure 1-3 – Field distribution in a solenoid (left) and a permanent magnet (right)

The field is only uniform in the centre of the coil, making accessibility an issue, and high fields require high currents. As we increase the field strength, losses due to these currents quickly lead to overheating problems.

Figure 1-4 – A liquid nitrogen cooled solenoid. Most of the space is occupied by the cooling coils!

We can improve things by using a coolant such as liquid nitrogen, which makes the system even larger, or by using a superconducting coil. Such systems work well, but are very large and expensive to maintain. A smaller, simpler system would have clear advantages. This project aims to look into a possible way of realising this aim using a "flux pump"

1.2 What is a thermally actuated magnetic system?

It sounds a bit of a mouthful – however, as the name suggests, it is a device that can pump magnetic flux from point A to point B. In doing so it should be possible to create an area of controllable flux density of almost arbitrary strength[4], as suggested by Dr. Tim Coombs, the supervisor for this project. From here on, this proposed system will be referred to as a TAS.

1.2.1 How could it work?

We can do this by using a material with a variable permeability. A higher permeability material will tend to concentrate the flux of an applied field. If this high permeability area can be moved, then so can the magnetic field. We can achieve this merely by holding a block of iron under a magnet – under the high permeability iron, the flux density will be increased over the local value. However, this is not much help – we have no way of "offloading" this flux and causing it to accumulate. Anything we move from A to B moves back again when we remove the block. What we need is a way of moving our block inwards, without its removal completely reversing what we have achieved.

If for instance we have a circular disk of material and can produce a toroidal area of high permeability moving inwards from the outer edge then we have such a situation. We could do this with a material whose magnetic properties were temperature dependant. As with any permanent magnet, the maximum field around this toroidal area will be at the edges. So as the toroid moves inwards towards the centre, we observe a peak of magnetic field tracking with the leading edge towards the centre.

Crucially however, if the permeability then drops from the outer edge inwards, the trailing edge is still moving towards the centre – the system is not symmetrical, so rather than reversing the flux pump, it actually repeats it in the same direction:

---

[4]   GBP290529 "Superconducting Systems"

1) Heating up from the outer edge:

Axis of rotation

Illustration of flux density above material as thermal wave progresses

COLD	HOT

Direction of thermal wave
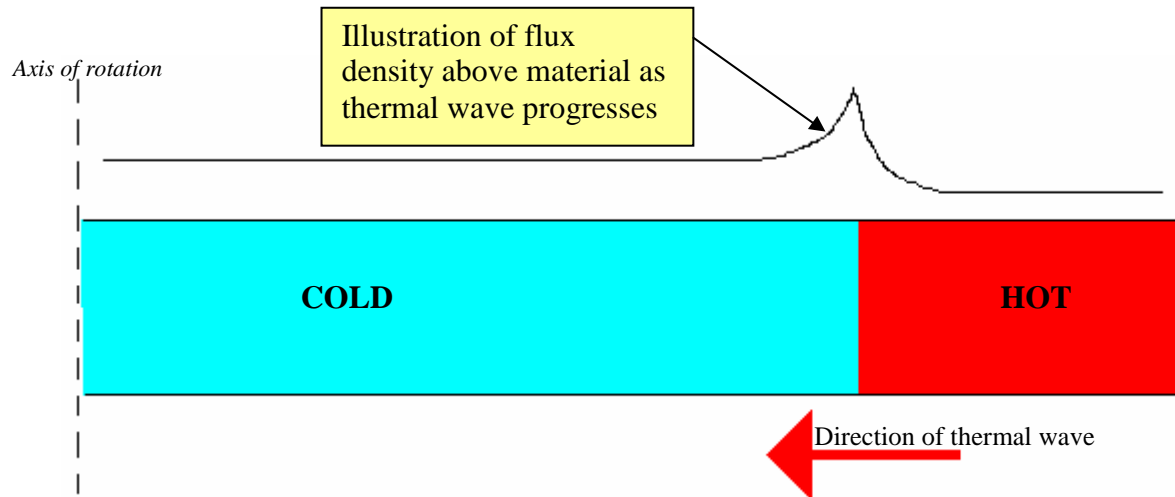
First, a heat pulse is applied at the outer edge of our cylinder. As the heat pulse moves inwards, the permeability falls. Due to flux concentrations at the boundary between hot and cold, we get a pronounced peak moving in towards the centre.

2) Cooling down from the outer edge:

Axis of rotation

Illustration of flux density above material as thermal wave progresses

HOT	COLD

Direction of thermal wave
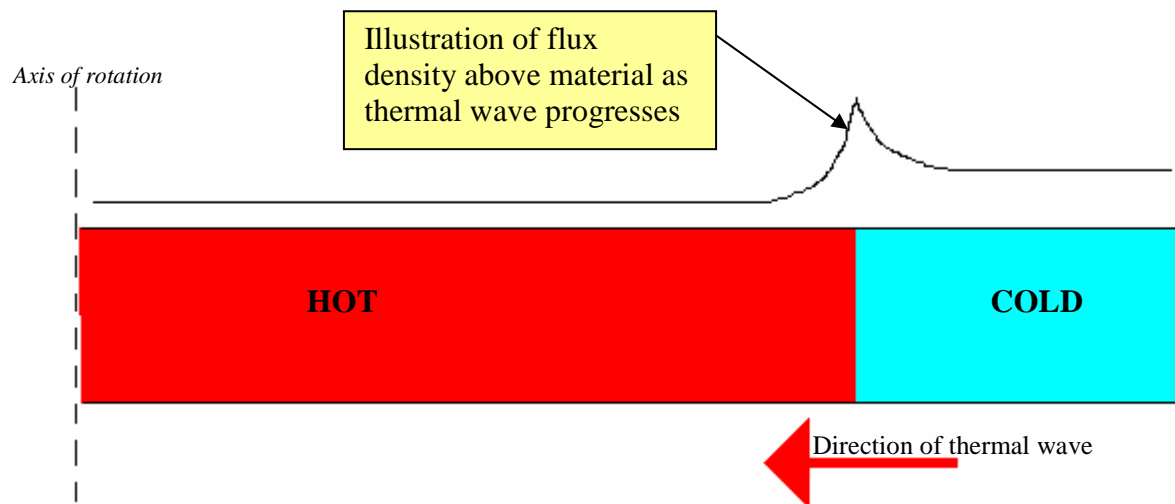
Figure 1-5 – Magnetic wave creation

When the heat pulse is turned off, the sample cools from the outer edge inwards. Again we have a magnetic pulse moving inwards – the key is that the peak due to flux concentrations appears at the boundary between high and low permeability. Although the boundary is reversed, the direction of travel is not.

2 Introduction to superconductivity

The previous section introduced the idea behind a TAS. While a way has been suggested of "pumping" flux from point A to point B, so far no method has been suggested for keeping it there.

To find a solution to this problem, it is necessary to make use of superconducting theory, and the following section will give a brief introduction to the basics to ensure grounding for later sections of the report.

2.1 What is a superconductor?

A superconducting material is a material that exhibits zero resistance to current flow. Almost all conductors exhibit a drop in resistance with falling temperature – and many will exhibit a change to a superconductor at some critical temperature, T_c.

This was first observed in 1911 by Heike Kamerlingh Onnes in Mercury. He was studying the resistivity of the material, and noticed that it disappeared completely and abruptly at a T_c of 4.2K.
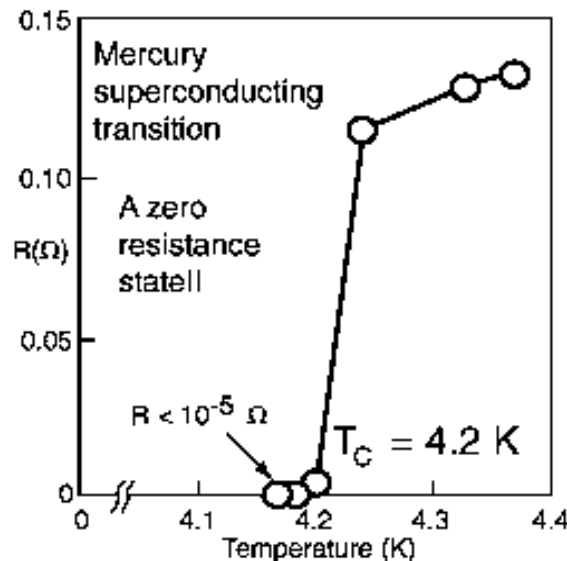
Figure 2-1 – Superconducting transition temperature

We will start by considering a "perfect" superconductor – called a type I superconductor:

If a conductor is placed in a changing magnetic field – i.e. $\dfrac{dB}{dt} \neq 0$

Then according to Lenz's law[5] a current will be induced in that conductor whose sense is such so as to create a magnetic field that opposes the field that created it[6]. This is the basis behind screening of electrical wires – induced currents in the shielding prevent the penetration of an externally applied field to the wires inside the sheath.

However, in a standard conductor, there is some resistance, and the blocking effect is not perfect – some energy is dissipated as heat due to the induced currents.
In a perfect conductor, there would be no losses due to heat, and so complete blocking of applied field. We would have a perfect diamagnet.

However, it should be noted that a superconductor and a perfect conductor are not quite the same. The differences become apparent when considering how the field is applied.

---

[5]   Formulated by German physicist Heinrich Friedrich Emil Lenz in 1833
[6]   This is obvious if conservation of energy is considered. If the sense of the current were reversed, then the applied field and the conductor would tend to accelerate towards each other, generating increasingly large currents in the conductor, and increasingly large amounts of kinetic energy – we would have made energy!

Zero-field cooled

If we make our conductor into a perfect conductor in the absence of any applied field, then apply a field, the material will experience a non zero dB/dt, and so currents will be induced to block this field entirely.

Likewise, if we have a superconductor in its superconducting state, and then apply a field, we will have currents induced to block this field, and again zero field penetration
So in the zero field cooled case, a perfect conductor and a superconductor behave the same.
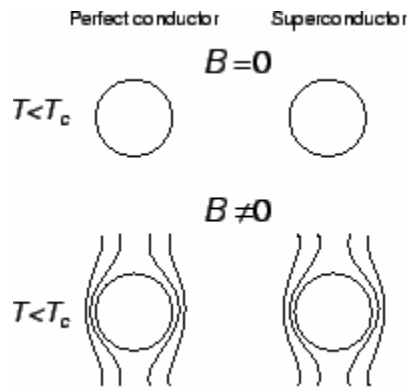
Figure 2-2 – Zero field cooling

Field cooled

The difference only becomes apparent when we look at the field cooled case. First let's look at a perfect conductor: If we apply a constant field to a conductor, which then loses all resistance, then the field will continue to penetrate. There has been no dB/dt since entering the zero resistive state, and hence no blocking currents created. If the external field is removed however, as the external field is removed currents are induced to oppose this motion, and the material is magnetized in opposition to the original field.

If however we apply a field to a type I superconducting material in its "normal" (non superconducting) state, and then make it superconducting, all flux will be expelled (as long as the applied field is less than the critical field for the superconductor – above which it is driven normal)
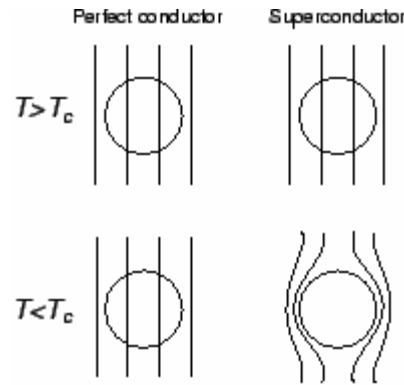
Figure 2-3 – Field cooling

This expulsion of flux even in the field cooled state can not be explained using our basic understanding of a changing flux inducing a current – there is no changing flux in this case. The effect is referred to as the Meissner effect[7]

2.2 The Meissner effect

The Meissner effect can be modelled with reference to Maxwell's laws and to the London equation.

The London equation relates the curl of the current density inside a superconductor to the magnetic field in the same material:

$$\vec{\nabla} \times \vec{J} = \frac{-1}{u_o \lambda_L} \vec{B}$$

where J is the current density in the material, λ_l is the penetration depth of the magnetic field, and u_o is the materials permeability.

We can combine this with one of Maxwell's equations:

$$\nabla \times B = u_o J$$

$$\vec{\nabla} \times \vec{\nabla} \times \vec{B} = -\nabla^2 \vec{B} = \vec{\nabla} \times u_o \vec{J} = \frac{-1}{\lambda_L} \vec{B}$$

$\nabla^2 B$ is the Laplacian of B. In one dimension this can be written as:

---

7   Discovered by Walther Meissner and Robert Ochsenfeld in 1933 ("Ein Effekt bei Eintritt der Supraleitfahigkeit", Naturwissenschaften)

$$\nabla^2 B = \frac{dB^2}{dx^2}$$

Thus in one dimension we have:

$$\frac{dB^2}{dx^2} = \frac{-1}{\lambda_L} B$$

This differential equation has a solution of the form:

$$B(x) = B_o e^{\frac{-x}{\lambda_L}}$$

Where B_o is the field at the boundary ($x=0$)

From this it can be seen that as x increases, B(x) falls, with the rate of falloff dependant on the penetration depth λ_L. Although this has been illustrated for 1D, similar results would be observed for 3d geometries.

This shielding of the applied magnetic field from the bulk of the material is what is known as the Meissner effect.

2.3 Type I and II superconductors

2.3.1 Type I superconductors

A type I superconductor is what we have been considering so far. Our superconductors have not allowed any field to penetrate, behaving as perfect diamagnets. If the applied field rises above a critical field, H_{c1}, they become normal. It becomes a superconductor below a certain critical temperature. It will remain in a superconducting state unless one of the following occurs:

- The applied field is greater than some critical field, H_c
- The current density in the material rises above some critical limit, J_c
- The temperature rises up again above the critical temperature, T_c
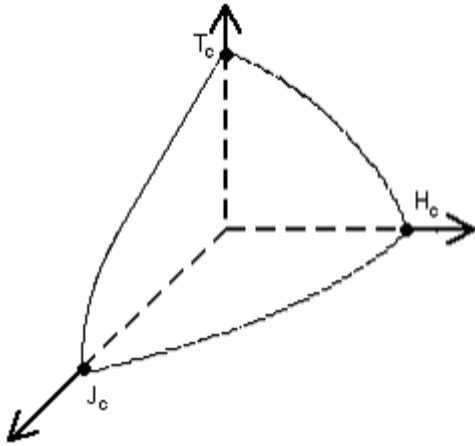
Figure 2-4 – The enclosed area shows where superconducting behaviour is observed

While superconducting, the Meissner effect ensures no flux penetration into the material (below the penetration depth) – it is in the Meissner state. Surface currents flow which block the applied field. We will show later that the current density in a superconductor is always either zero, or J_c, the critical current density. The higher the applied field, the more current needs to flow to block it, and for a given critical current density the space needed for this current increases, so the penetration depth rises. Ultimately, the applied field is such that even with a penetration depth equal to the depth of the sample itself the shielding can not be maintained, and the sample goes normal. These type of materials are classed as "soft" superconductors, and were the first to be discovered.

2.3.2 Type II superconductors

While Type I superconductors will go straight from superconducting to normal state at a certain applied field, H_{c1}, a type II superconductor will first enter a transition state. It does so at H_{c1}. At a higher field still, H_{c2}, it will become normal. In this transition state, the material is still superconducting, but some flux lines can penetrate the material.
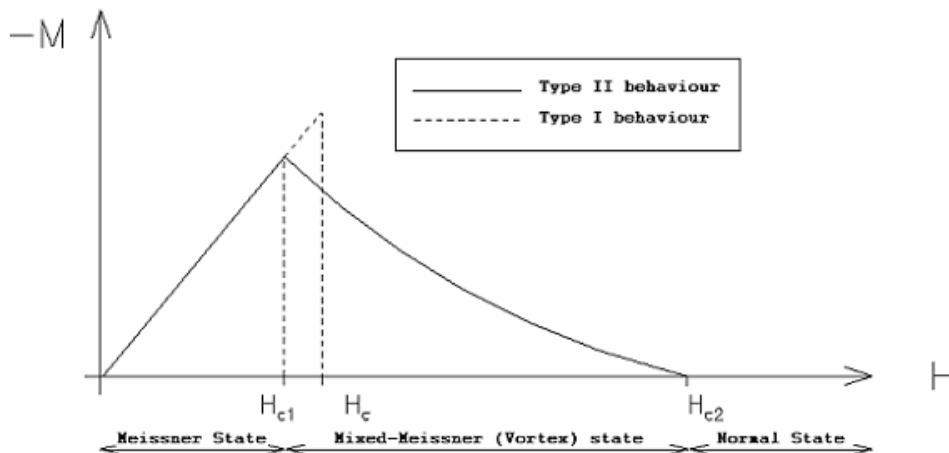
Figure 2-5 – Type I and Type II superconductors

2.3.3 Mixed Meissner State

The existence of a mixed state is what differentiates a type II from a type I superconductor. The critical field at which the type II superconductor becomes normal, H_{c2}, is generally far higher than H_c / H_{c1}. For most uses therefore, type II superconductors are far more useful, as the fields we can work with are much higher. There are other advantages of type II superconductors however. With a pure type I superconductor, all applied field is expelled. This would appear to lead to levitation – trains, bearings, etc. However, in fact it is unstable – even with carefully constructed geometries, there is at least one direction in which the levitating object can escape. If however we use a type II superconductor, then we have some flux penetration (hence the "mixed" state) This flux passes through normal regions of the superconductor, and is pinned in place by the surrounding material, which is still superconducting. Thus we have the levitation effect of the Meissner state, plus stability due to the pinned flux.

Figure 2-6 – A combination of the Meissner effect (Type I) and flux pinning (Type II) gives us stable levitation

In more detail, the following is how this pinning occurs. The penetrating field induces surface currents to shield it from the rest of the material, but this time the surface currents flow around the flux, giving us a vortex of current. However, critical current is a function of applied field – as applied B rises, the critical current density falls – if the applied field is too great, the critical current falls such that the shielding currents exceed J_c, and the material again goes normal. The flux lines themselves are pinned within the vortices – if they attempt to move out, the effect is cancelled by the currents. If we can also pin the vortices themselves, then we can fix the field. Pinning of the vortices can be achieved by careful material design, introducing microscopic pinning centres into the material.
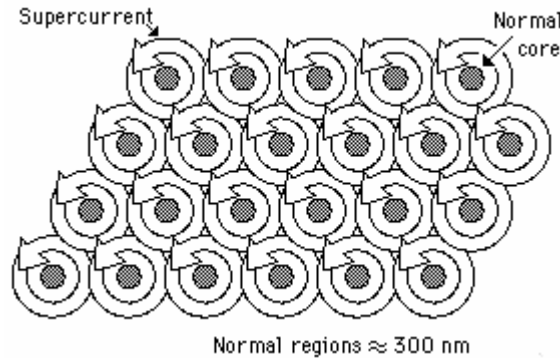
Figure 2-7 – Current vortices around flux lines

2.4 Critical state models

Having introduced the basic theory of superconductivity, it is worth looking at the critical state models used to describe this superconducting behaviour. There are two main models to choose from:

- Bean [8] (critical current density is Jc everywhere that B penetrates)
- Kim [9](critical current density is a function of applied field, B)

Of these three, the simplest and most commonly used is the Bean model. For the purposes of this report it will be sufficient, and will be the only one discussed here.

2.4.1 Bean model

The bean model makes use of the fact that the onset of the superconducting state is very rapid – it goes from resistive to completely non-resistive almost instantaneously. Current is a function of resistance, and with no resistance, in the presence of an applied field the screening current will increase to the critical current density immediately on application of an external field. Any further increase in current would drive the material normal – and simple "path of least resistance" states that the current will expand inwards into the superconductor rather than increasing above J_c so long as there is any superconducting material left. If is only once shielding currents have reached the centre of the sample that an increased field may drive the superconductor normal. However, even here there will be some leeway – once full current penetration has occurred, the applied field can increase significantly before the material is finally driven normal. And in fact, in order to achieve a residual field once the applied field has reduced to zero, the applied field must be at least twice that needed to cause complete penetration of the shielding currents. This is best illustrated using diagrams:

---

[8] "Magnetization of High Field Superconductors" - Physical Review, 1964
[9] "Critical Persistent Currents in Hard Superconductors" – Physical Review 1962

$$\frac{dB}{dx} = \mu_0 J_c$$

1

Initially a field, B, is applied. As the field attempts to penetrate the material, we have a dB/dt, which induces currents to oppose this field. Because we have a superconductor, there is no resistance to current flow, and the current density will be equal everywhere to the critical current, Jc.

As the applied field strength rises, it penetrates further into the bulk, and more current is induced to block it. Eventually a field is reached such that field just penetrates into the centre of the material.

2

As the flux starts to fall, from the outside in, currents are again induced – this time to oppose the falling of the flux within the superconductor – hence the direction of the induced currents is reversed.

Figure 2-8 - If the applied field is too low, there is no remnant field

B

M/μ0

+Jc

0

-Jc
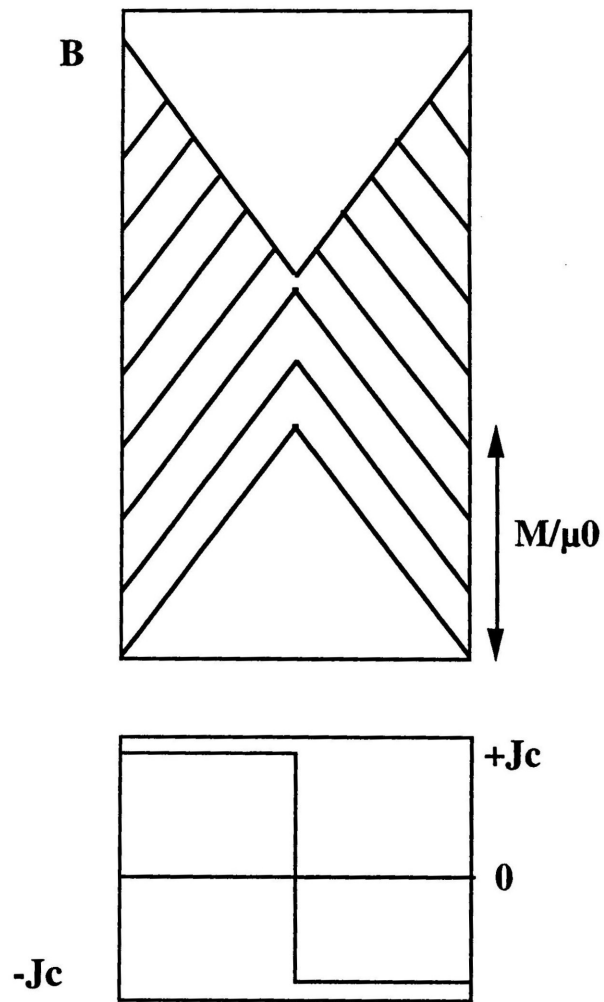
Figure 2-1: …if the applied field is greater than B, we retain a remnant field. 2B gives the maximum possible remnant field

3

If however we apply a field greater than that needed to just penetrate the bulk, then we do have a net field once the original field has been removed. As the applied field rises above B, so we begin to see a remnant field.

The figure above shows an applied field of 2B. As the applied field falls, the shielding currents are completely reversed, leaving a net field, corresponding to the maximum field that can be trapped in the material.

3 Using superconductors in a TAS

It was described in an earlier section how a moving magnetic wave could be produced using a material whose magnetic properties were temperature dependant (see *Figure 1-5*, page 5)

If we link this in with the superconducting theory introduced above, we can describe the full system:

We have three layers to our system, the magnet, the variable permeability layer (actuated by heat), and the YBCO superconducting layer.
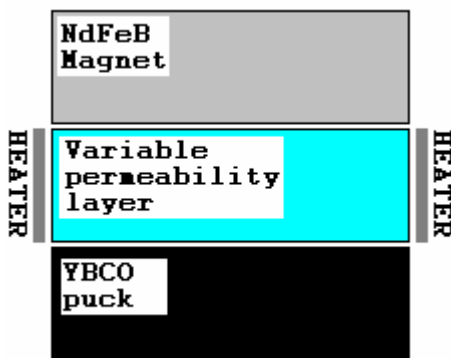
Figure 3-1 – The three layers of our proposed setup

1)
Initially, we have our variable permeability layer in a high permeability state all over. The field from the magnet is less than H_{c1}, so there is no flux penetration of the YBCO puck.

2)
We heat up the edge of the variable permeability material, sending a toroidal pulse of heat towards the centre. This produces a toroidal ring of low permeability. At the transition between high and low permeability, we see a concentration of flux lines

3)
This crowded flux density is higher than H_{c1}, so overcomes the Meissner effect and penetrates into the bulk of the material

4)
As the heat pulse moves inwards, so does the leading edge between high and low permeability, and thus so does the area of high flux density.
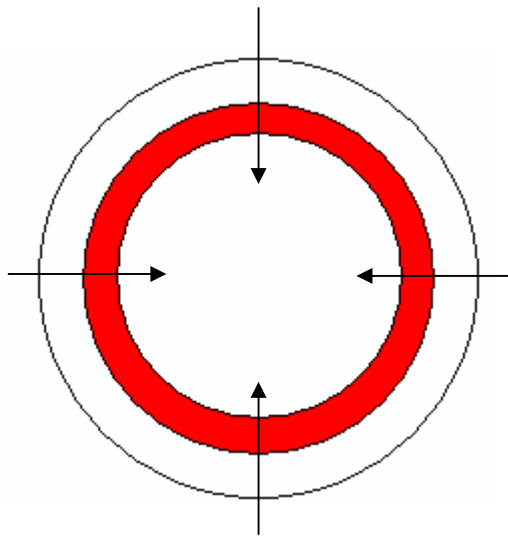
As we heat the edge of the variable permeability material, we send a toroidal ring of high permeability towards the centre of the puck.

This creates a toroidal ring of high flux density moving towards the centre

5)
Meissner shielding at the edge of the YBCO where the flux is not so concentrated prevents the flux from passing straight through the YBCO however. Instead it is dragged over the top surface, only penetrating slightly into the bulk.

6)

As these flux lines move towards the centre of the puck, we have a $\frac{dB}{dt}$, and so currents are induced in the superconductor. In front of the advancing flux a current is produced in a sense so as to impede the advance of the flux, while behind the advancing flux a loop is induced in the opposite sense to prevent the flux from moving away (Faraday's law)
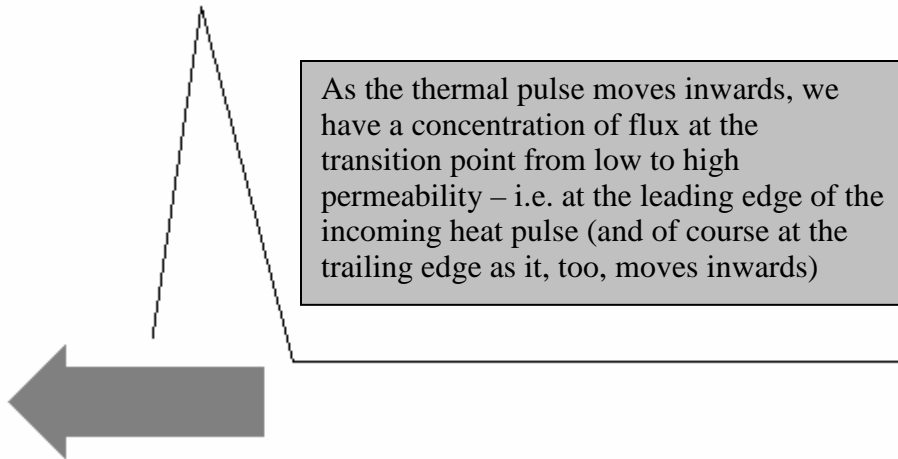
As the thermal pulse moves inwards, we have a concentration of flux at the transition point from low to high permeability – i.e. at the leading edge of the incoming heat pulse (and of course at the trailing edge as it, too, moves inwards)

7)

As the flux moves forward, the trailing current loops are left flowing, while the leading current loops are wiped out by the advancing flux. Eventually we have a current loop in one direction throughout the material, except for the very centre (which never gets covered by the advancing flux) where the current sense is opposite.
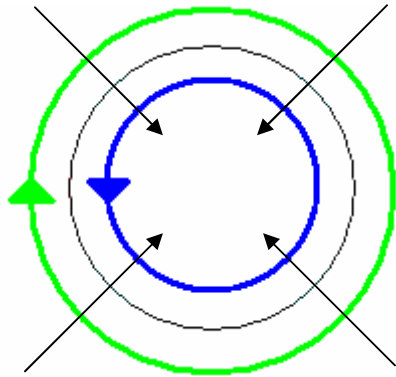
The centre lie represents the peak of the magnetic wave created by the leading edge. As it moves inwards, current loops (blue) are induced to oppose it. Meanwhile at the trailing edge of the peak, currents are induced to prevent the wave from moving onwards. The inner (blue) currents are wiped out as the toroidal ring shrinks, leaving the green currents flowing.

8)

When the leading edge reaches the centre, it vanishes (the entire sample is now hot). Without this edge, there is no concentration of flux, and the flux lines from the magnet revert to their original positions

9)

While the flux lines were dragged in through the surface of the YBCO, they are free to "snap" back again, so the process of current induction is NOT reversed, and we have a net current loop induced in the material.

10)

We can then start to cool our material from the outer edge inwards

11)

Again, we have a leading edge moving inwards, but this time the hot/cold boundary is reversed

12)

However the direction of the concentrated flux stays the same

13)

So again, we get more currents induced in the YBCO

14)

As we repeat the process more and more times, we get a larger build up of current, and a larger resultant field. Because the resultant field is caused by the trailing edge currents, induced to try to prevent the decrease in flux as the peak moves by, the resultant field is in the same sense as the applied field,– and we have a TAS!

4 Simulated TAS using FEM

Having started off with the basic idea for a TAS as outlined in the introduction, it was first necessary to test the concept. To do this, a FEM model was designed[10]. This modelled the following situation:

- Axially symmetric layer of variable permeability material placed above a type II superconductor
- Magnetic field applied perpendicular to both surfaces
- "pulse" of high permeability sent inwards across the variable permeability material
- Process repeated

It was hoped that such a simulation would show a build up of current in the YBCO as the pumping continued, and this is what the model in fact showed. Each new numbered diagram below corresponds to a new pulse that has been applied to the material, showing the resultant fields and currents.
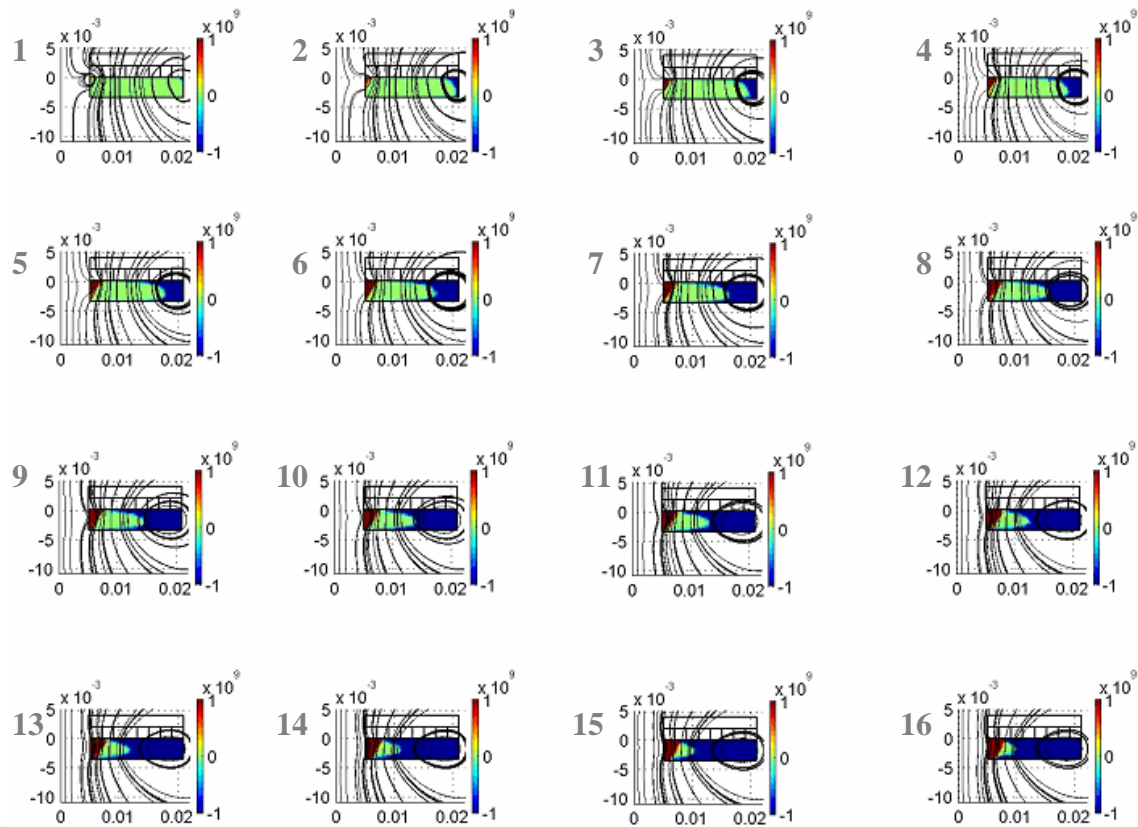
Figure 4-1 – Simulation of a TAS, courtesy Z. Hong

> *The above model is based upon axisymetric geometry. Horizontal axis show distance from the centre. The left hand axis shows thickness in meters. The right hand colour key shows the magnitude and sense of currents flowing within the material. So we can see that the dimensions of the simulated sample are approximately 3mm deep by 2mm radius. This is slightly wider and thinner than that which we produced in the lab, but is similar enough to be comparable.*

---

[10]   Z. Hong

The above figure shows a three layer axisymetric model: first a permanent magnet, then a layer of variable permeability material, then a layer of YBCO[11] superconductor. The Prussian blue has been split up into 8 cells, and each is "switched" from its low to its high permeability state in turn, starting from the outside (right hand) edge and moving inwards. The process continues until all 8 cells are high permeability, at which point the sequence repeats, but with low permeability filling in, again from the right hand side.

The images show a series of times though the simulation, and read from left to right. Each numbered image represents another pump that has been applied.

During each pump, as this thermal wave moves inwards, the leading edge induces currents so as to oppose the advancement of this leading front. Meanwhile, the trailing edge of the magnetic wave induces currents in the opposite sense so as to oppose the disappearance of the wave. As the wave progresses inwards, the currents induced by this leading edge are "overwritten" by those induced by the trailing edge. The net result is that we have a series of current loops in the same sense induced by the trailing edge (the blue areas), and only a small number of loops flowing in the opposite sense in the very centre, where the trailing edge never passes (red area). Because the blue area is far larger than the red, we have a net field.

In our simple model of a superconductor, any currents that flow in a superconductor flow at the critical current density Jc. As pumps are repeated, more sheilding currents are produced. The initial currents can't increase, so new currents start to flow further inside the bulk of the material. Thus we can see that as the process is repeated (moving from one pump at the top left to 16 at the bottom right) these currents move further and further into the material, until all of the material is carrying current in one sense or the other, and the material is saturated.

We might expect the shielding currents to move downwards from the top surface as the applied field increases. However, it must be remembered that our applied field is not uniform – it is stronger at the edges that at the centre. So it is to be expected that we should see greater penetration at the edges of the sample. In this case the applied field is such, coupled with the dimensions of the puck, that the edges are completely saturated from the first pump.

Note that the currents induced by the leading edge are seeking to prevent the advancement of the magnetic wave, so create a magnet of the opposite polarity to the applied field. The trailing edge induces a field to resist the disappearance of the magnetic wave, and so creates a magnet of the same polarity to the applied field, and it is this field which remains. A consequence of this is that the applied field is reinforced with each pump, so with each successive pump the effect is greater. This can clearly be seen on the following plot, generated from the simulation discussed above:

---

[11]   Yttrium barium copper oxide, HTS with $Tc \approx 85K$
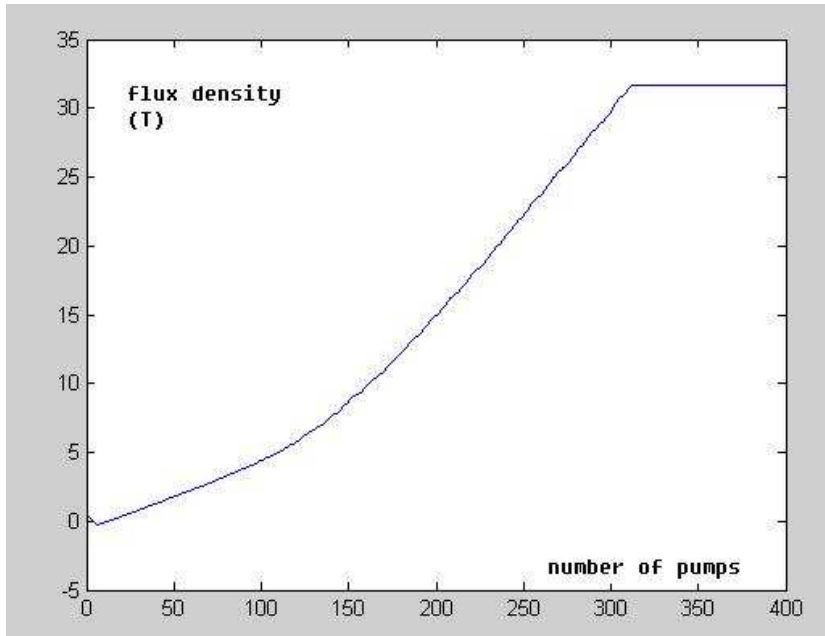
Figure 4-2 – Resultant flux density with number of pumps (courtesy Z. Hong)

The simulation was run with an initial applied field of only 20mT using a superconductor with a critical current density, Jc, of 1e10A/m^2. Based on the sample dimensions, this critical current gives a saturation field of the order of 30T as shown. However, because the initial field is so weak many hundreds of pumps are required to reach saturation. It can be seen though that the increase is not linear, due to the reinforcing effect of the induced field on the total applied field.

5 Prerequisites of real world implementation

5.1 Prussian Blue

The idea surrounding the basics of a TAS have been outlined, and it has been shown using a simulation that the idea should work in practice.

However, it was still necessary to find a method for realising a toroidal, shrinking ring of high permeability. A material was needed with variable, controllable permeability. The solution that was found was Prussian Blue and its analogues – first used as dyes at the start of the 18th century[12]. Used initially as a bright blue pigment – the first such stable compound that had been available to artists, it is the compound's magnetic properties that are of interest here.

---

[12]   In 1704 by a Berlin draper named Diesbach discovered by chance a recipe to make a new blue pigment useful for paints and fabrics. This discovery was reported anonymously in 1710 and the recipe itself was described in 1724 by Woodward and Brown

After a search of published works, the following plot for a Nickel Chromium analogue was found[13]:
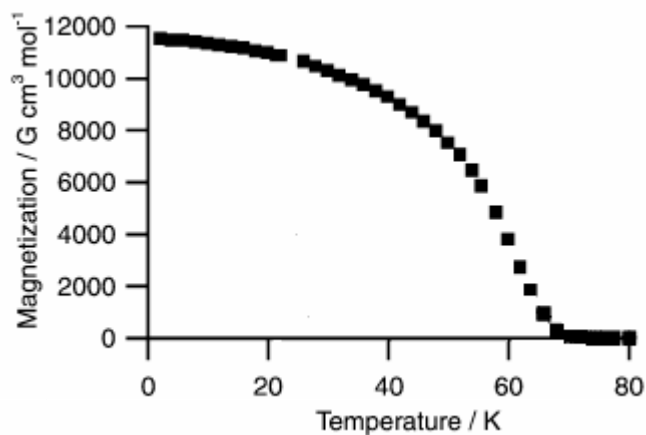
Figure 5-1 – Ferromagnetic transition of $Ni_{1.5}^{II}[Cr^{III}(CN)_6]$

This analogue showed a significant, reversible change in magnetic properties with temperature. Further research indicated that the entire Prussian blue family exhibits such properties at various temperatures and to various extents.

5.1.1 Magnetic Properties

It was found in 1928 by Davidson and Wilo that Prussian blue -

 - exhibited a change from paramagnetic to long range ferromagnetic behaviour at a curie temperature[14], T_c of 5.6K[15]. This is the kind of change we are looking for – a way of moving from a high to a low permeability state and back again.

Furthermore, it has been shown that various Prussian blue analogues exhibit similar behaviour. A number of these analogues are shown below, along with their Tc values:

Analogue		Tc (K)
$Cr^{III}V^{II\,[a]}$	$KV[Cr(CN)_6]\cdot 2\ H_2O$	376
$Cr^{III}V^{II}/V^{III}$	$K_{0.058}V[Cr(CN)_6]_{0.79}(SO_4)_{0.058}$	372
	$K_{0.50}V[Cr(CN)_6]_{0.95}\cdot 1.7\ H_2O$	350
	$V[Cr(CN)_6]_{0.86}\cdot 2.8\ H_2O$	315
	$V[Cr(CN)_6]_{0.69}(SO_4)_{0.23}\cdot 3.0\ H_2O$	315
$Cr^{III}Cr^{II}$	$[Cr_5(CN)_{12}]\cdot 10\ H_2O$	240
$Mn^{II}V^{II}$	$(Et_4N)_{0.5}Mn_{1.25}[V(CN)_5]\cdot 2H_2O$	230
$Cr^{III}Cr^{II}$	$Cs_{2/3}Cr[Cr(CN)_6]_{8/9}\cdot 4.4\ H_2O$	190
$V^{II}Mn^{II}$	$Cs^2\ Mn[V(CN)_6]$	125
$Cr^{III}V^{IV}$	$(VO)[Cr(CN)_6]_{2/3}\cdot 3.3\ H_2O$	115

---

[13] Chem-Comm : "Ion-exchange synthesis and magneto-optical spectra of colored magnetic thin films composed of metal(II) hexacyanochromates (III)"

[14] The temperature above which all ferromagnetic behaviour is lost

[15] "New Magnetic Functionalities presented by Prussian Blue analogues" – Electrochemical society Interface, Autumn 2002

$Cr^{III}Mn^{II}$	$CsMn[Cr(CN)_6]$	90
	$(NMe_4)Mn[Cr(CN)_6]$	59
$Mn^{IV}Mn^{II}$	$Mn[Mn(CN)_6] \cdot 1.14\ H_2O$	49
$Co^{II}Co^{II}$	$Co_3[Co(CN)_5]_2 \cdot 8\ H_2O$	38
$Mn^{II}Mn^{II}$	$K_2Mn[Mn(CN)_6]$	41
$Mn^{III}Mn^{II}$	$CsMn[Mn(CN)_6] \cdot 0.5\ H_2O$	41
	$(NMe_4)[Mn_2(CN)_6]$	28
$Mn^{II}Mn^{III}$	$Mn_3[Mn(CN)_6]_2 \cdot 12\ H_2O$	37
	$Mn_3[Mn(CN)_6]_2 \cdot 12\ H_2O \cdot 1.7\ CH_3OH$	29
$Mn^{III}Mn^{III}$	$Mn[Mn(CN)_6]$	31
$Mn^{III}V^{III}$	$V[Mn(CN)_6]$	28
$Mn^{III}Cr^{III}$	$Cr[Mn(CN)_6]$	22
$Fe^{III}Co^{II}$	$Co_3[Fe(CN)_6]_2$	14
$Fe^{III}Mn^{II}$	$Mn_3[Fe(CN)_6]_2$	9
$Fe^{III}Fe^{II}$	$Fe_4[Fe(CN)_6]_3 \cdot x\ H_2O$	6
$Fe^{III}Ni^{II}$	$Ni_3[Fe(CN)_6]_2$	24
$Mn^{III}Ni^{II}$	$Ni_3[Mn(CN)_6]_2 \cdot 12\ H_2O$	30
	$CsNi[Mn(CN)_6] \cdot H_2O$	42
$Cr^{III}Ni^{II}$	$Ni_3[Cr(CN)_6]_2 \cdot 9\ H_2O$	60
	$CsNi[Cr(CN)_6] \cdot 2\ H_2O$	90

It would seem logical to simply choose an analogue with a high T_c, near to that of room temperature to facilitate easy investigation. However, the T_c value is not the only consideration is choosing a material. We need a substance with a transition over a narrow temperature range, and exhibiting the largest possible change in permeability on either side of the boundary. On top of this, it must be considered that while there are advantages to a high T_c, any experiment we design is going to involve superconductors - and even HTS such as YBCO have critical temperatures around 80-90K. Based on this fact, an ideal material would have a rapid transition at its curie temperature, high change in permeability, and a Curie temperature around the same as the critical temperature of our superconductor.

Having taken account of these considerations and through discussions with our colleagues in the chemistry department, it was decided to start investigations using a Nickel analogue of Prussian blue:

$$Ni_{1.5}^{II}[Cr^{III}(CN)_6]$$
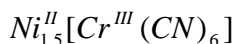
This analogue has a transition temperature of around 60K[16], and it was hoped would exhibit a rapid and large change in magnetic properties either side of this transition.

The expectation of a large change in permeability on either side of our critical temperature came from a paper found during our initial research[17], and its findings are outlined below.

---

[16]   ChemCom 2003 – "Ion-exchange synthesis and magneto-optical spectra of colored magnetic thin films composed of metal(II) hexacyanochromate(III)"

[17] ChemComm : "Ion-exchange synthesis and magneto-optical spectra of colored magnetic thin films composed of metal(II) hexacyanochromates (III)"
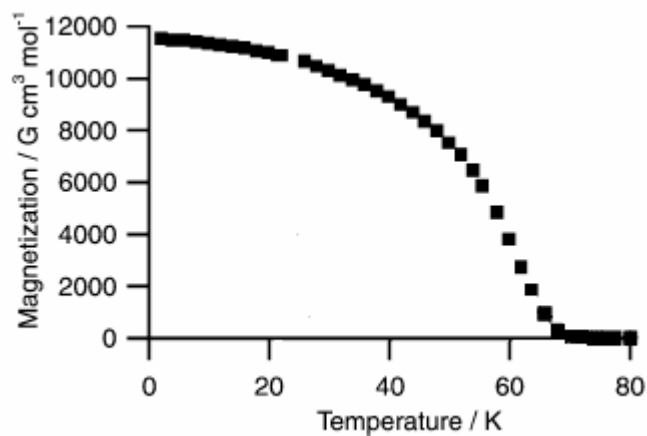
Figure 5-2 – Ferromagnetic transition of our analogue

The molecular weight of the analogue is 266.8
So 1 mole of the material weighs 266.8g

$$G = \frac{emu}{cm^3}$$

$$\therefore$$

$$Gcm^3\Big/mole = emu\Big/mole$$

At 50K, half way through the transition, the magnetization is approximately

$$7000 \; Gcm^3\Big/mole = 7000 \; emu\Big/mole$$

1 mole = 266.8g

The density of the analogue is approximately 1.56g/cm^3 (see page 33, "Density")
So 1 mole has a volume of 266.8/1.56 = 171.0 cm^3

So the expected magnetization is thus:

$$7000 \; emu\Big/171cm^3 = 40.93 \; emu\Big/cm^3 \; = \; 40929 \; A/m$$

This occurred in an applied field of 10G.
In CGS units, B=H

Thus 10G corresponds to a magnetising force of 10 Oe

$$10 \, Oe = 10 \times \frac{1000}{4\pi} = 795.77 \; A/m$$

Thus relative permeability is given by $u_r = 1 + \dfrac{M}{H} = \mathbf{52}$

So across the transition, a reasonably large change in relative permeability should be observed.

5.1.2 Chemistry of Magnetic Properties

A brief description of the chemistry behind the magnetic properties of Prussian Blue and its analogies will now be given, to help the reader understand the basis of our work. It should be noted however that this is an engineering paper, not a chemistry one, and that more detail on the processes involved can be found elsewhere[18]. The chemical equation for Prussian blue is:

$$4Fe^{3+}{}_{(aq)} + 3[Fe^{II}(CN)_6]^{4-}{}_{(aq)} \rightarrow \mathbf{Fe^{III}{}_4[Fe^{II}(CN)_6]_3}$$
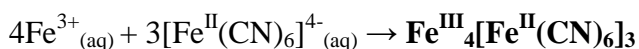
The magnetic properties arise from the interaction between the Fe^{II} and Fe^{III} ions within the material. If we examine the electron shell structure of the two Iron ions we find that:

Fe   [Ar] $3d^6 4s^2$

Electrons will be lost from the outer shells first, so for the iron ions in question we have:

Fe^{II}   [Ar]$3d^6$
Fe^{III}   [Ar]$3d^5$

The magnetic properties of the ion depend on the electron pairing within the valence shells. If we have unpaired electrons, then we will have a paramagnetic behaviour. Depending on the interactions between individual ions, this may give us a paramagnetic bulk material (if there is little interaction between the electron alignment of the individual ions), or ferromagnetic behaviour, if there is a greater interaction.

All electrons in a given electron shell will have the same energy level, and so we might expect there to be no electron pairing in the valence orbitals (of which there are five in the d level). The electrons would spread out as far as possible from one another. While this would be the case in an isolated ion, in a molecule such as our Prussian blue the bonds to the rest of the molecule can distort these outer shells in a process known as orbital-splitting.

---

18   See footnote [x] on following page
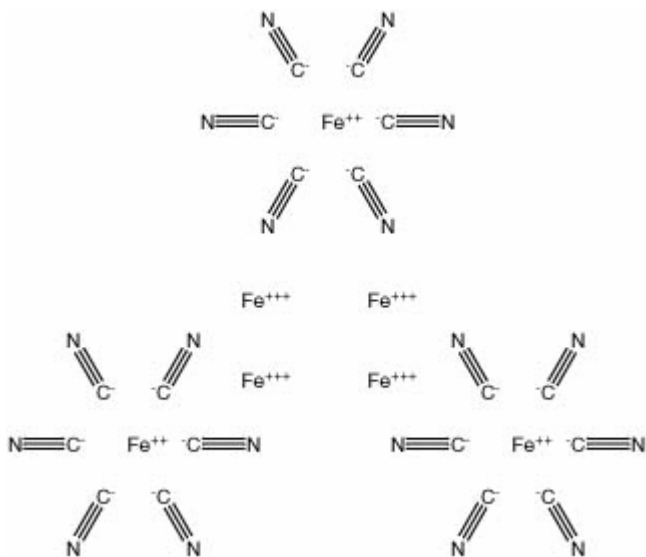
Figure 5-3 – Chemical structure of $Ni_{1.5}^{II}[Cr^{III}(CN)_6]$

Prussian blue is an ionic compound.
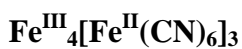
$Fe^{III}_4[Fe^{II}(CN)_6]_3$

So each Iron^{III} ion is surrounded by 3 $[Fe^{II}(CN)_6]_3$ in a tetrahedral structure. Internal to the $[Fe^{II}(CN)_6]_3$ each Fe^{II} ion is surrounded by 6 CN$^-$ ions. Thus we have 18 positive charges, and 18 negative, and thus the charges balance.

The valence electrons of the Fe ions are all in the d orbital, the sub-orbitals of which take the following orientations:
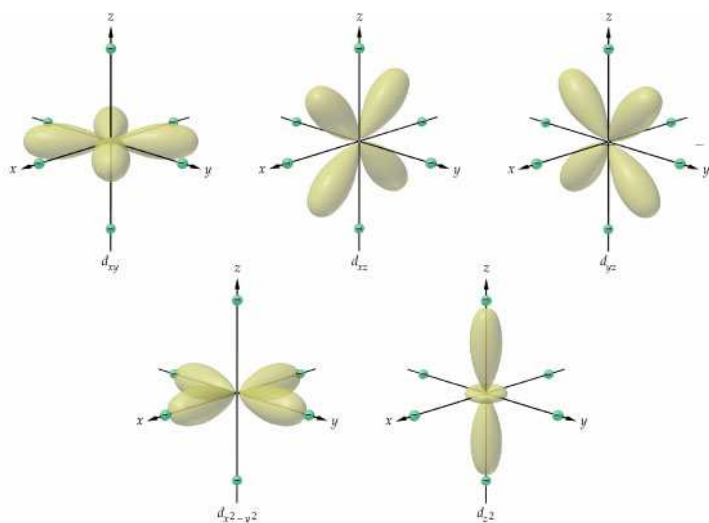
Figure 5-4 – d- sub-orbitals

Fe^{II}

Our Fe^{II} ions are surrounded by 6 CN$^-$ ions in an octahedral arrangement. These ions arrange themselves along end of each of the x, y, and z axes. In doing so, the presence of these ions will distort these d sub-orbitals. The orbitals are no longer all at the same energy level – those aligned directly with the CN ions are repelled, so these orbitals rise up in energy. By conservation of energy, so that there is no net change, the remainder must be shifted to a slightly lower energy level. Of the 5 d orbitals, two were involved in bonding, 3 not. So our split is 2 increases, and 3 decreases in energy levels:
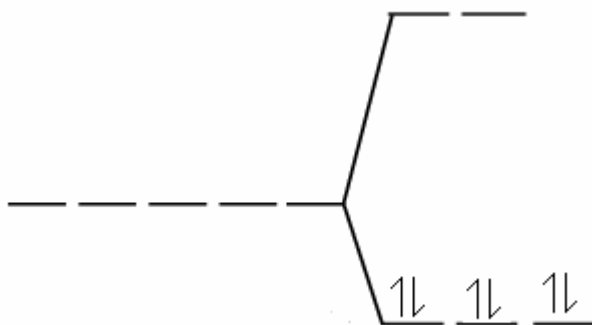
Figure 5-5 – Crystal level splitting in Fe^{II}

There is an energy cost in pairing up two electrons in an orbital, since like charges repel. However, it can be seen that there is also an energy cost in placing electrons into the higher of the split energy states. We will not examine the detailed chemistry here, but suffice to say the energy balance means that in this case it is energetically favourable for three paired electrons to fill the lower of the split energy levels.

Because all electrons are paired, there is no net magnetic moment. Hence this part of the molecule is diamagnetic (it is not completely non-magnetic, as there will be some realignment of electron orbitals in the prescience of an external field that will oppose it)

Fe^{III}

Our four Fe^{III} ions are surrounded by three (Fe(CN)^6)$^{4-}$ ions. It is less obvious how these 3 ions will distribute themselves around our four Fe^{3+} ions.

Whereas in the previous case with an octahedral field we had each ion pointing directly at an orbital, here that is no longer the case. There is no direct alignment between ions and sub-orbitals, and as a result, the split we observe is less than in the octahedral case. Three orbitals are raised up in energy, while three are forced into a lower energy state to compensate.
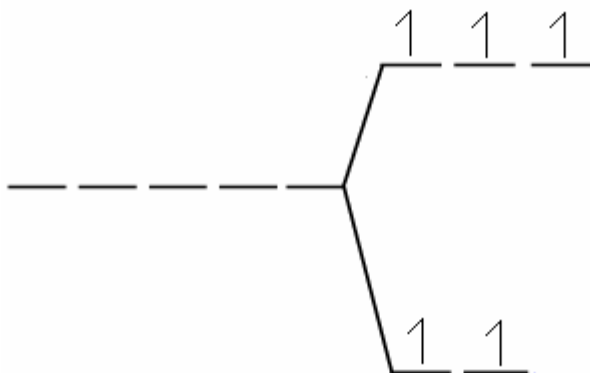
Figure 5-6 – Crystal level splitting in Fe^{III}

In the previous case pairing electrons was energetically favourable to splitting them across energy levels. Here, however, the energy split is less, because no ligands point directly at orbitals. Thus in this instance, the energy costs associated with pairing up electrons and the energy levels of the split itself mean that it is favourable for all electrons to have their own orbital.

So Fe^{III} has 5 unpaired electrons, and thus a net magnetic moment - it is paramagnetic.

This combination of paramagnetic Fe^{III} interspersed with diamagnetic Fe^{II} ions. For ferromagnetic behaviour to be observed, we must have long range ordering between our Fe^{III} ions. Because of their large separation however, very little thermal energy is needed to disrupt this long range order – hence the low curie temperature of 5.6K.

If however we can make use of one of the analogues of Prussian blue where both ions are paramagnetic then we can expect a far higher curie temperature- and the stronger the paramagnetic behaviour of the ions involved, the higher the curie temperature will be.

Taking the analogue we have been examining:

$$Ni_{1.5}^{II}[Cr^{III}(CN)_6]$$
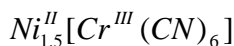
In this case the energy costs of pairing electrons versus the split energy levels mean that both the Ni and the Cr ions have unpaired electrons, and so both are paramagnetic. Thus the thermal energy needed to disrupt the long range ordering between the ions is greater, and the curie temperature is correspondingly higher at around 60K. Various combinations of transition metals will produce various transition temperatures depending on the interaction between their electron structures, which we will not go into further here. If more detail is required, there are a number of chemistry papers that would be worth examining[19].

---

[19]   "Electrons at work in Prussian Blue Analogues" – the electrochemical society interface, autumn 2002

"Is it possible to Get High TC Magnets with Prussian Blue Analogues? A Theoretical Prospect" Chemistry –a European journal volume 11, issue 7 , Pages 2135 - 2144

5.1.3 Superparamagnetic behaviour

The above discussion holds true for materials with large particle size, over about 10nm. However, below this size we may see a phenomenon called superparamagnetism.

As has been discussed, the Curie point of a material denotes that temperature below which the thermal energy is insufficient to overcome ferromagnetic coupling between atoms within the material, and so ferromagnetic behaviour is displayed. However, if our crystal sizes become small enough, then it can be the behaviour of the individual crystals as a unit rather than their constituent atoms that affect behaviour. The thermal energy may be too low to disrupt long range ordering at the atomic level, but it may still be sufficient to change the direction of magnetization of the entire crystal. The energy needed to accomplish this is the crystalline anisotropy energy, and is size dependant. Eventually it will drop below the energy needed to disrupt coupling between atoms, and thus the bulk material will exhibit paramagnetic behaviour even below its curie temperature.

If we are preparing our Prussian blue samples as a powder, then fine powders are an advantage in that they exhibit high packing factors, and thus can easily be pressed into pucks, with the small particle and high packing factor meaning they can hold themselves together via Van der Walls forces. However, it must be considered that if the particle size is too small, we risk destroying our ferromagnetic transition as our material becomes superparamagnetic.

As an aside, it should be noted that this is a significant problem for data storage. If we are using individual particles magnetic polarization to store data, such as on a hard disk drive, then the smaller we can make those particles, the higher our data density. However, if the particles become too small, they become superparamagnetic as opposed to ferromagnetic, and no longer retain their data (they merely align with any external field). This limit is known as the superparamagnetic limit, and is causing serious problems for disk designers.

6 Synthesis

If a layer of a Prussian blue analogue with a suitable transition temperature from Ferro to paramagnetic can locally be heated across that temperature range, then we have our variable permeability material. It was thus necessary to investigate the ways of producing this material.

6.1.1 Crystal growth

A paper was found which discussed the possibilities of growing a layer of Prussian blue crystals on a layer of substrate of Nafion[20].
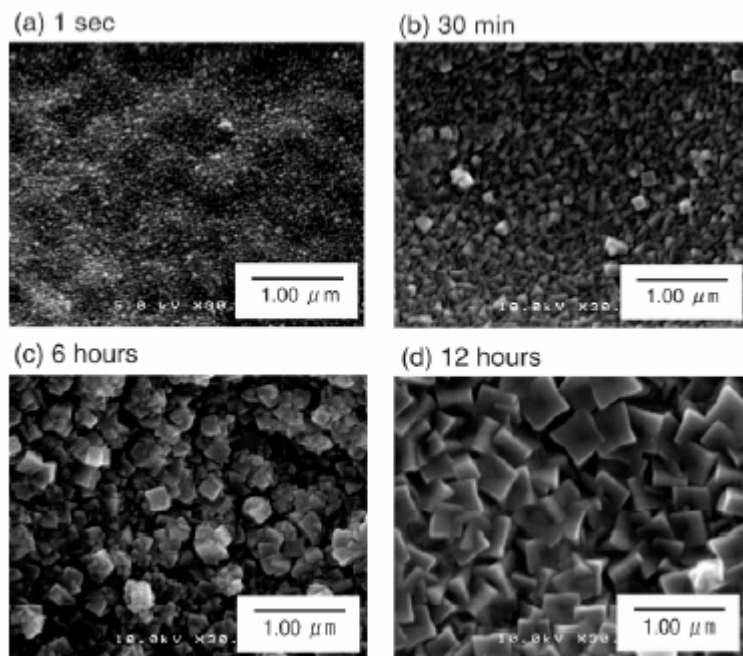
Figure 6-1 – SEM images of crystal growth on a Nafion^{TM} membrane

In the above figure the crystal growth that the authors obtained can be seen.
A number of attempts were made to replicate this procedure. Some growth was seen (although the SEM resolution was limited). However, the surface was not homogeneous. There is also an issue with the thickness of the layer. Our TAS relies on a changing permeability material. As the permeability changes, so the field distributing locally changes. However, any such material would be part of a magnetic circuit, and such a thin layer would make very little difference to that circuit, making any changes in field tiny away from the material itself. However, details of what we obtained are shown below:

---

[20]   "Ion-exchange synthesis and magneto-optical spectra of colored magnetic thin films composed of metal(II) hexacyanochromate(III)" – ChemComm 2003
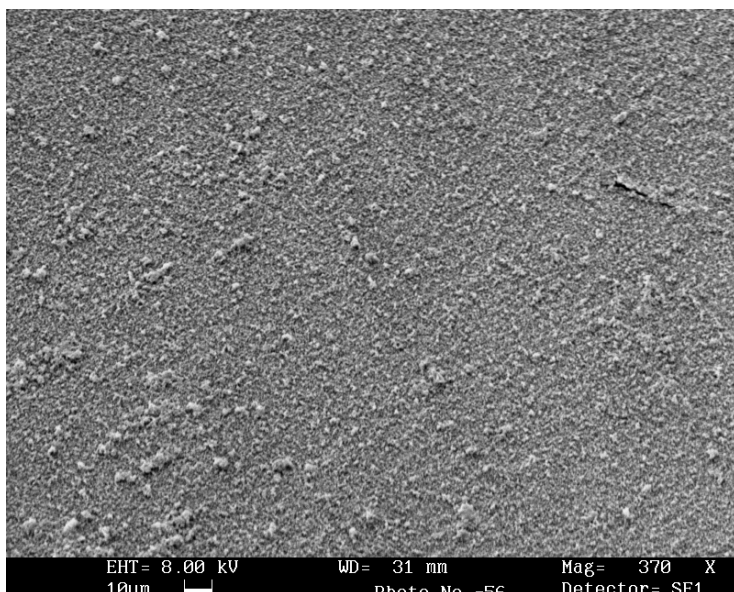
Figure 6-2 – Our own SEM images of attempted crystal growth

The above image shows the surface of our membrane. It can be seen that there has been some growth across the surface – at this zoom level it is hard to see exactly what this growth is though, although it does not appear to be homogeneous.
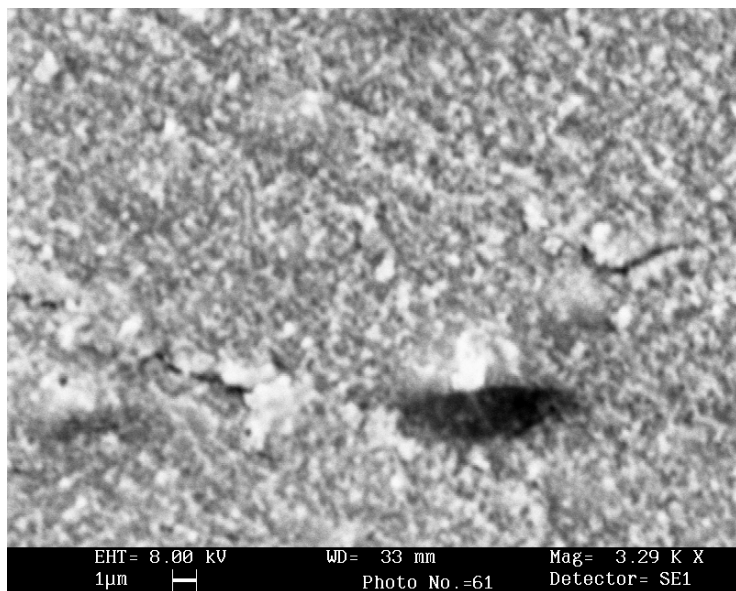
Figure 6-3 – A closer view proves elusive, but again the surface appears non homogeneous, and not at all similar to the images produced in the paper.

Based upon the images from the paper included above, at this zoom level individual crystals ought to be visible. While there is a large body that could be a crystal, most of the surface is sill covered in very small particles.

6.1.2 Powder precipitate

It was decided that, in response to our difficulties in growing a thin film on a substrate, we would investigate the possibilities of producing a basic powder form of Prussian blue, which could then be formed into solid pucks. Making a powder of the analogue proved trivial:

The analogue in question was

$$Ni_{1.5}^{II}[Cr^{III}(CN)_6]$$
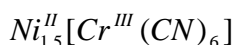
The procedure for producing this in powder form used precursors in the following ratios:

- Dissolve $NiCl_2$ (1.5 mol) in the minimum amount of water and
- Add to a concentrated solution of $K_3[Cr(CN)_6]$ (1mol) in water.
- $Ni_{1.5}[Cr(CN)_6]$ precipitates from the solution over 20 min.
- The gelatinous precipitate is filtered off
- Precipitate is dried in a vacuum dessicator for 24-48 hrs or longer.
- Powder can then be removed from dessicator and stored. Some caking may occur, necessitating careful use of a pestle and mortar to break up the particles, while taking care not to crush them completely.

6.1.3 Puck

The powder as formed was coarse and difficult to work with. In any working system a way would be needed of forming the powder into a useable solid. Having discarded the idea of growing a layer of crystals onto a substrate (see page 30), attempts were made to press it into a puck using a die and press. However this caused disintegration of the crystals, and risked leading to super-paramagnetic behaviour (see page 29). A solution was to make use of a binding agent. As a first attempt, we used "Silverdag^{TM}", which is a suspension if silver particles in an organic solvent. Once the solvent has evaporated, we are left with a solid silver mass made up of many tiny silver particles, and these tiny particles can fill the gaps between our crystals, and keep the sample together. These pucks were prepared with the minimum volume of "Silverdag^{TM}" to produce a cohesive solid – optical images of the surface as prepared are included below:
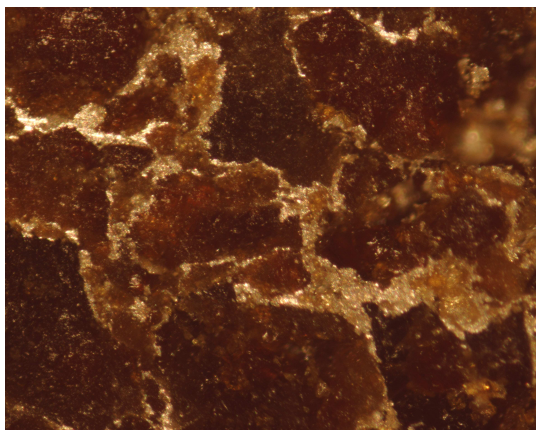
Figure 6-4 – Surface of puck magnified x50

Various pressures and silver / solid ratios were tried during the initial stages. In determining the volume of silver to be used, a number of factors had to be considered:

- More silver gives better structural strength
- More silver means less magnetic material, so less change in permeability for the bulk
- Our permeability change is thermally actuated. Although the Silverdag™ is not solid, but made up of a mass of close fitting particles, its presence is almost certain to increase the thermal conductivity of the sample, which will thus affect how we can actuate the system.

The above image shows the structure of one of the final pucks. Now that a way of preparing bulk samples of our magnetic material had been found, the next step was to check that the magnetic properties of the material were as good as was expected.

6.2 Density

Knowing the density of our material is also useful. A paper was found that had analysed the crystal structure of another analogue of Prussian blue[21]:

$$NaMn[Cr(CN)_6]$$

Which is similar to our Nickel analogue:

$$Ni_{1.5}^{II}[Cr^{III}(CN)_6]$$
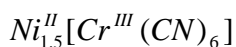
This paper gave the structure and size of the unit cell – that is the smallest repeating structure within the crystal - and from this calculated density. If we make the assumption

21 Dong et al., "A Prussian Blue Type Ferrimagnet Na[MnCr(CN)6]: Single crystal structure and magnetic properties"

that the crystal structure and size is the same in our analogue[22], then we can calculate density values for our analogue also:
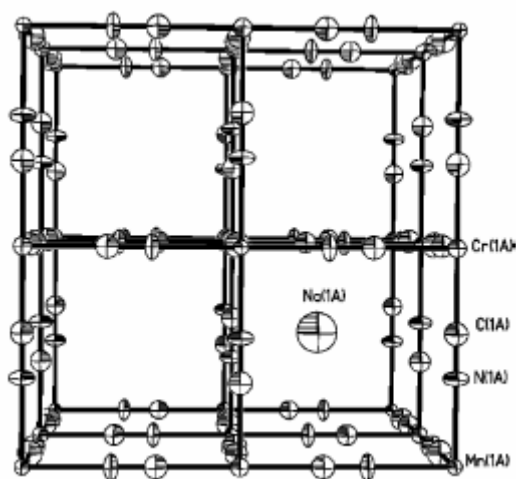
Figure 6-5 – Crystal structure of $NaMn[Cr(CN)_6]$

The unit cell has sides of $a = b = c = 10.8159\text{Å}$

The unit cell thus has a volume of $abc = 1.2653 \times 10^{-21} cm^3$

The unit cell contains 4 molecules of our analogue

The molecular mass of our analogue is 296.14g/mol

1 mole contains 6.02×10^{23} molecules (Avogadro's constant)

Thus one unit cell weighs:

$$\left(\frac{4}{6.02 \times 10^{23}} \right) \times 296.14 = 1.9677 \times 10^{-21} g$$

Giving a density of:

$$\frac{1.9677 \times 10^{-21} g}{1.2653 \times 10^{-21} cm^3} = 1.56 g / cm^3 = 1560 Kg / m^3$$

---

[22]   A reasonable assumption, according to colleagues in the chemistry department

7   Characterisation of materials to be tested in experimental setup

Having prepared samples of Prussian blue in both powder and puck form, it was necessary to check on the magnetic properties of our material. Making use of a SQUID[23] magnetometer, which measures the magnetization of a sample in response to an applied magnetic field at a user defined temperature, the variation of the samples magnetic properties were recorded, and the results obtained are presented below.

F*igure 7-1 – Close of Prussian Blue analogue puck*

SQUID measurements

7.1.1 Correction for demagnetization factor

It was necessary to characterise the magnetic properties of the analogue that had been produced. However, the measured magnetization of any given sample is dependant on that samples geometry. This is due to the self cutting of the sample by its own flux lines. These flux lines will oppose the magnetic domains that created them, and the overall resultant field is reduced. This reduction due to self-cutting is quantified by the use of a "demagnetization factor", N, where $0 \le N \le 1$

The effect of this self-cutting is best described using diagrams:

---

[23]   Superconducting Quantum Interface Device. Enables measurement of magnetic moment to be made under varying field and temperature conditions.

A long, flat plate magnetized perpendicular to its long axis will have a near unity demagnetization factor, as all flux passes through the body
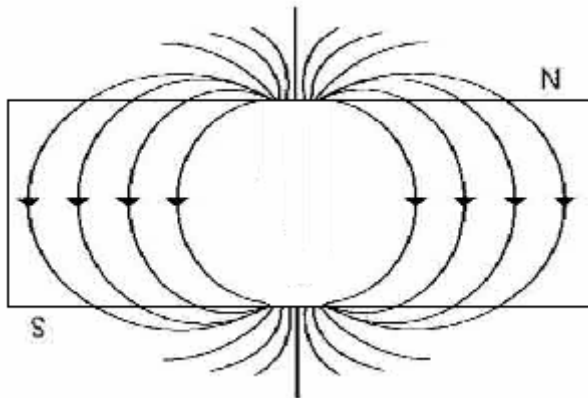
Figure 7-2 – A thin, flat magnet has a great deal of flux cutting

Conversely, a long, thin rod will have a near zero demagnetization factor, as there is practically no self-cutting
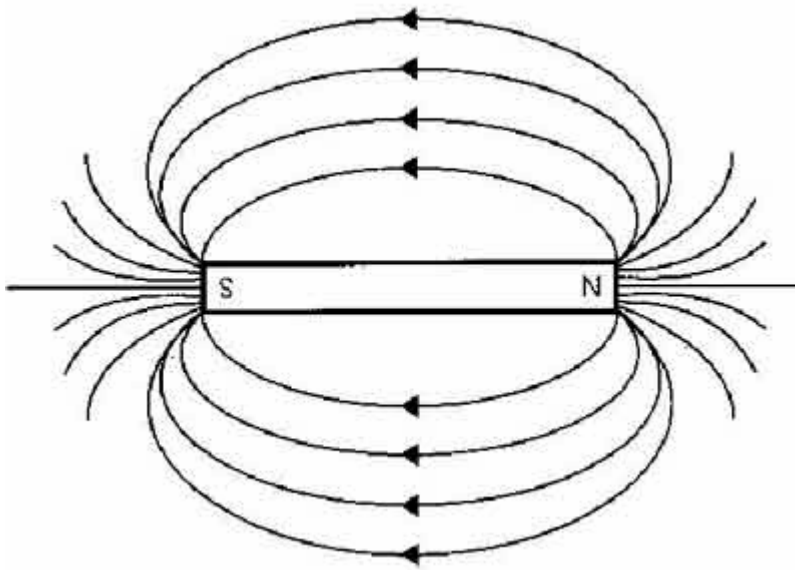
Figure 7-3 – …While a long, thin rod has very little

It can be seen from the above diagrams that certain shapes will give rise to high demagnetization factors, while others will give low values. However, if we are to obtain accurate results for the magnetization of our sample, independent of geometry, we need a way of quantifying these factors.

Calculating these values for any given geometry is a non-trivial problem. However, work has been done on calculating the figures for ellipsoids[24], from which we can obtain a good estimate of the values for our sample.

---

[24]   Demagnetizing factors of the general ellipsoid

The relevant equations for an ellipse with three ellipsoid semi-axis a,b,c are:

$$L = \frac{\cos\phi\cos\theta}{\sin^3\theta\sin^2\alpha}[F(k,\theta) - E(k,\theta)]$$

$$M = \frac{\cos\varphi\cos\theta}{\sin^3\theta\sin^2\alpha\cos^2\alpha}\left[E(k,\theta) - \cos^2\alpha F(k,v) - \frac{\sin^2\alpha\sin\theta\cos\theta}{\cos\phi}\right]$$

$$N = \frac{\cos\varphi\cos\theta}{\sin^3\theta\cos^2\alpha}\left[\frac{\sin\theta\cos\phi}{\cos\theta} - E(k,\theta)\right]$$

Where:

- N, L, and M are the demagnetization factors in the *a,b,*and *c* directions respectively
- $\cos\theta = c/a \quad (0 \leq \theta \leq \pi/2)$
- $\cos\phi = b/a \quad (0 \leq \theta \leq \pi/2)$
- $\sin\alpha = \left[\frac{1-(b/a)^2}{1-(c/a)^2}\right] = \frac{\sin\phi}{\sin\theta} = k$
- $F(k,\theta)$ and $E(k,\theta)$ are the elliptical integrals of the first and second kind. *k* is the modulus and θ is the amplitude of these integrals

The above has already been tabulated for us, and this table is included in appendix A of this report. The following plot shows the data is graph form. Note that the demagnetization factor has been scaled by $1/4\pi$ because the paper it was published in[25] used the CGS unit system.

---

[25] "Demagnetization factors for the general ellipsoid" March 24, 1945
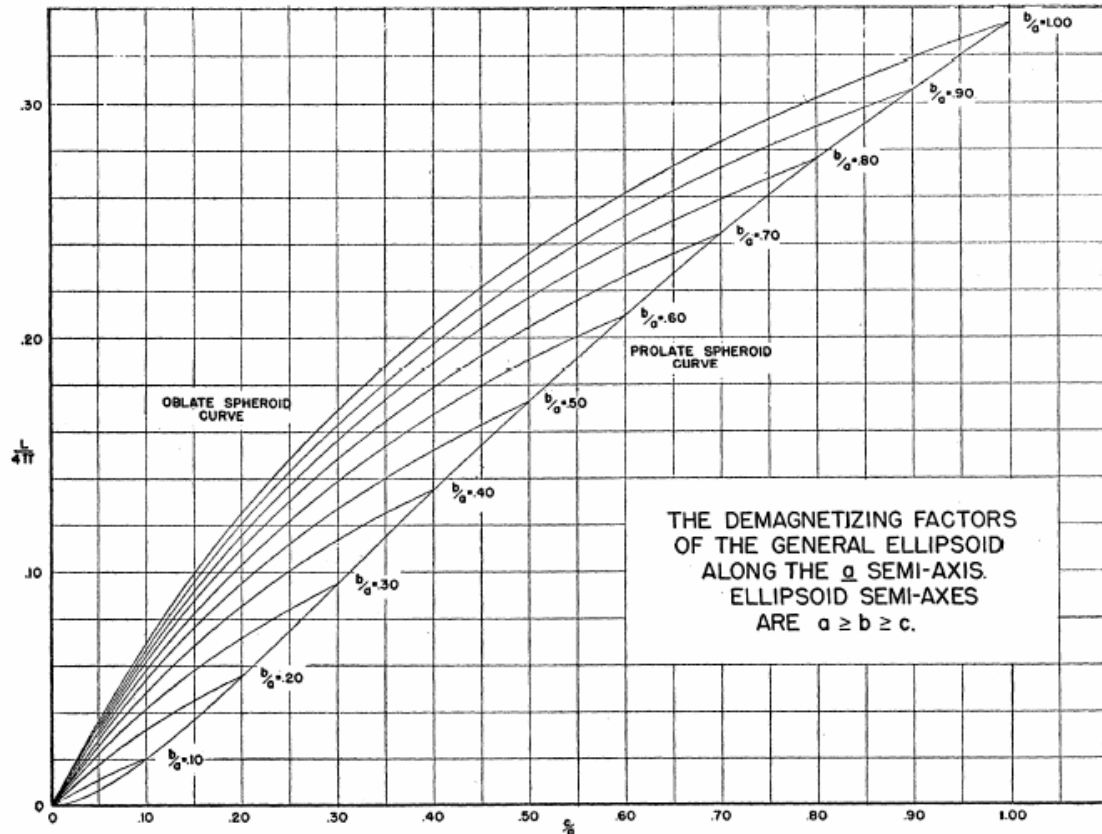
Figure 7-4 – Demagnetization factors for various geometries of ellipsoids

7.1.2 Packing Factor

To calculate the magnetic properties of the material, we not only need to take its volume into account, but also the amount of material present, so that the measured magnetization can be normalized for volume. In the case of the puck this is not an issue, as we can simply observe the behaviour of the material as a whole. However, when examining the raw powder, it does become an issue.

In the initial SQUID tests, the prepared powder was pressed down tightly into a gelatine pill capsule. Because of the large grain size, the packing factor was likely to be low, and the cigar shape of the pill casing made accurate volume measurements difficult.

7.2 SQUID Results

SQUID analysis was conducted of the initial Prussian blue analogue, both in powder form, and in puck form (with silver as a binder). The results from these analyses are discussed below.

7.2.1 Raw powder

Measuring the volume of a powder directly is non trivial. However, knowing its density, we can use its mass to calculate volume.

Internal Diameter	:	4.7mm
Total length	:	13.84mm

Thus internal volume :

$$\left[\pi \times \left(\frac{4.7}{2}\right)^2 \times (13.84 - 4.7)\right] + \left[\frac{4}{3} \times \pi \times \left(\frac{4.7}{2}\right)^3\right]$$

$$= 213mm^3$$

Figure 7-5 – Gelatine pill capsules used for mounting powder in the SQUID

Mass of Prussian blue	=	0.1816×10^{-3} Kg
Density of Prussian blue	=	1560 Kg/m^3[26]

$\therefore$

$$V_{PB} = \frac{0.1816 \times 10^{-3}}{1560} = 1.164 \times 10^{-7} m^3 = 116.41mm^3$$

This gave us a packing factor of $\dfrac{V_{PB}}{V_{capsule}} = 0.55$

Based upon the dimensions of the gelatine capsule, and approximating it as a prolate (cigar shaped) ellipse, we were also able to calculate the demagnetization factor as:

a	=	13.84mm
b=c	=	4.7mm
c/a=b/a	=	0.34

$N \approx 0.12$

The SQUID records a magnetization value. To obtain the material magnetisation we have to follow three steps:

Normalize for volume — *Divide reading by volume of sample multiplied by packing factor*

Correct for demag. factor — $H_{internal}=H_{applied}-NM$

---

[26] See "Density", page 33

Scaling our recorded magnetization as detailed above gave us the magnetization of the material itself, independent of geometry. This gave us the following plots for temperature vs. Magnetization and MH curves at various temperatures:
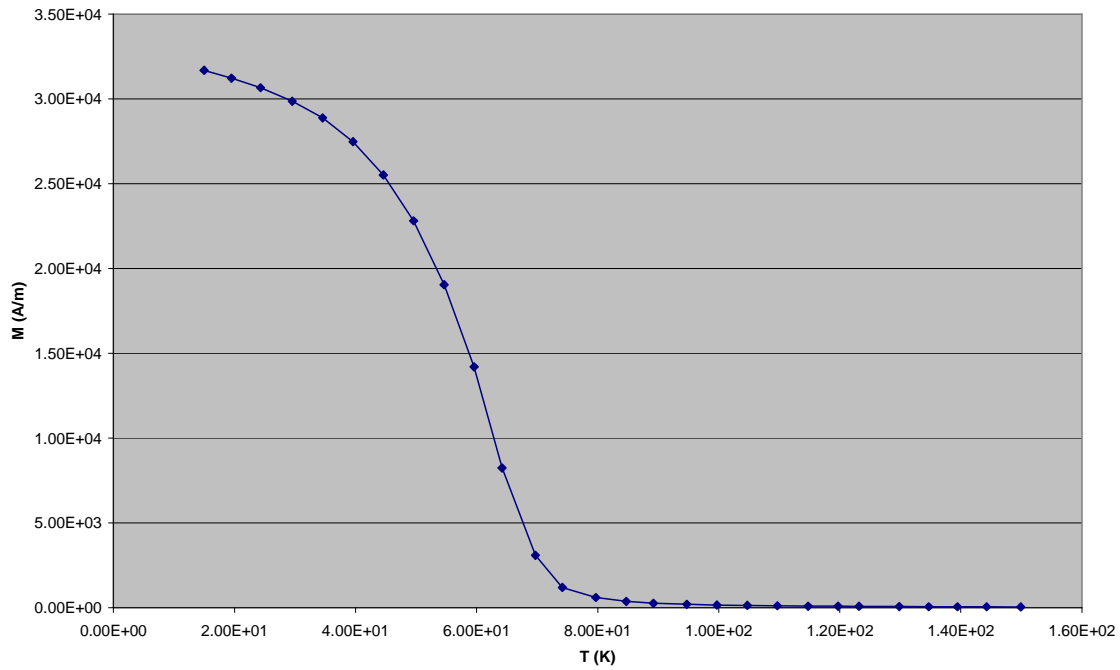
Figure 7-6 – Temperature vs. Magnetization for raw powder (data collected on the 20/11/2005)
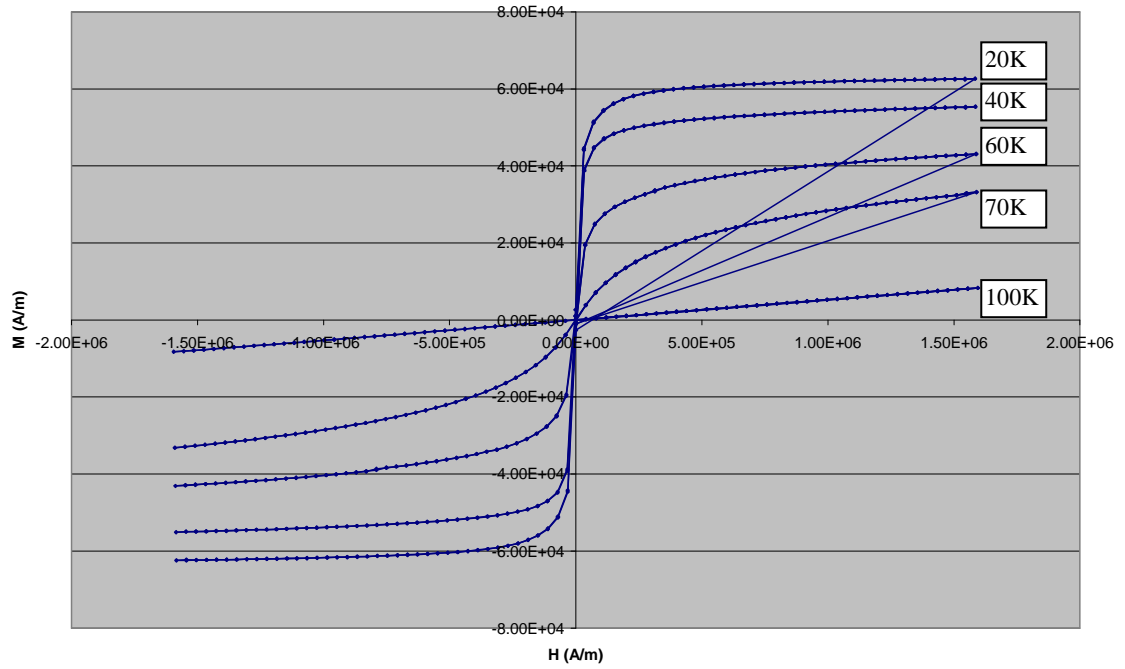
Figure 7-7 –MH curve for raw powder (data collected on the 20/11/2005)

The hoped for transition was seen at 60K. By examining the unsaturated portions of the MH plots at various temperatures, it was possible to extract the change in permeability across the transition:

$$M = \chi_v H$$
$$B = u_o (H + M) = u_o (H + \chi_v H) = u_o (1 + \chi_v) H = u_o u_r H$$

where:

$u_r = 1 + \chi_v$, and is the relative permeability of the material

But $\chi_v = \dfrac{M}{H}$, which is the gradient of our MH plot.

Below the transition:
$u_r \approx 1$
Above the transition,
$u_r \approx 3$

The change in permeability was not nearly as high as had been predicted (see page 22). However, the readings were repeated and found to be constant.

41

7.2.2 Puck SQUID results

Although the permeability was lower than anticipated, having tested the raw powder, we proceed to test our silver bound puck of the same material. The puck should give improved results over the raw powder, as the silver binder and the pressure under which the pucks were formed provides a far higher packing factor, and the well defined shape makes calculating volume and demagnetization factor simpler. To this end, the SQUID experiments were repeated, but with a puck segment in place of the gelatine capsule.

For the puck with silver binder, as discussed previously, the calculation is similar.

- We know the thermal properties of silver
- We know the density of the Prussian Blue powder (~1.56g/cm3)
- We know the mass of Prussian blue powder used in making each puck
- We know the density of silver
- We know the total volume of our puck

From this we can calculate the packing factor as follows:

$$\rho = \frac{m}{v}$$

$$\rho_{average} = (PF_{Ag} \times \rho_{Ag}) + (PF_{PB} \times \rho_{PB})$$

$$\rho_{average} = ((1 - PF_{PB}) \times \rho_{Ag}) + (PF_{PB} \times \rho_{PB})$$

$$\rho_{average} = \rho_{Ag} - (PF_{PB} \times \rho_{Ag}) + (PF_{PB} \times \rho_{PB})$$

$$\rho_{average} - \rho_{Ag} = PF_{PB}(\rho_{PB} - \rho_{Ag})$$

Where:

$$\rho_{average} = \frac{m}{v}$$

PF_{PB} =Packing factor (volume fraction) of the Prussian blue

PF_{Ag} =Packing factor (volume fraction) of the Silver

7.2.3   Giving us a packing factor of approximately:

$$\rho_{average} = \frac{m}{v} = \frac{1.221 \times 10^{-3}}{\pi \times (8 \times 10^{-3})^2 \times (3.87 \times 10^{-3})} = 1569.19 \, \text{Kg/m}^3$$

$$\rho_{PB} = 1560 \text{kg/m}^3$$

$$PF_{PB} = 0.99$$

This seems extremely high. It is likely that in fact it will be reduced slightly due to the fact that the silver is not solid, but a collection of tiny silver particles. It should also be noted that the packing factor will inevitable vary slightly from one puck to the next. However, the error introduced by this will hopefully not be great, and it is likely that the packing factor is in the high 90% range.

For the demagnetization factor we are interested in the value along the longitudinal axis,

a	=	14
b=c	=	3
b/a=c/a	=	0.21

$N \approx 0.056$

Using this packing and demagnetization factor applied to our squid data, the following plots were produced:
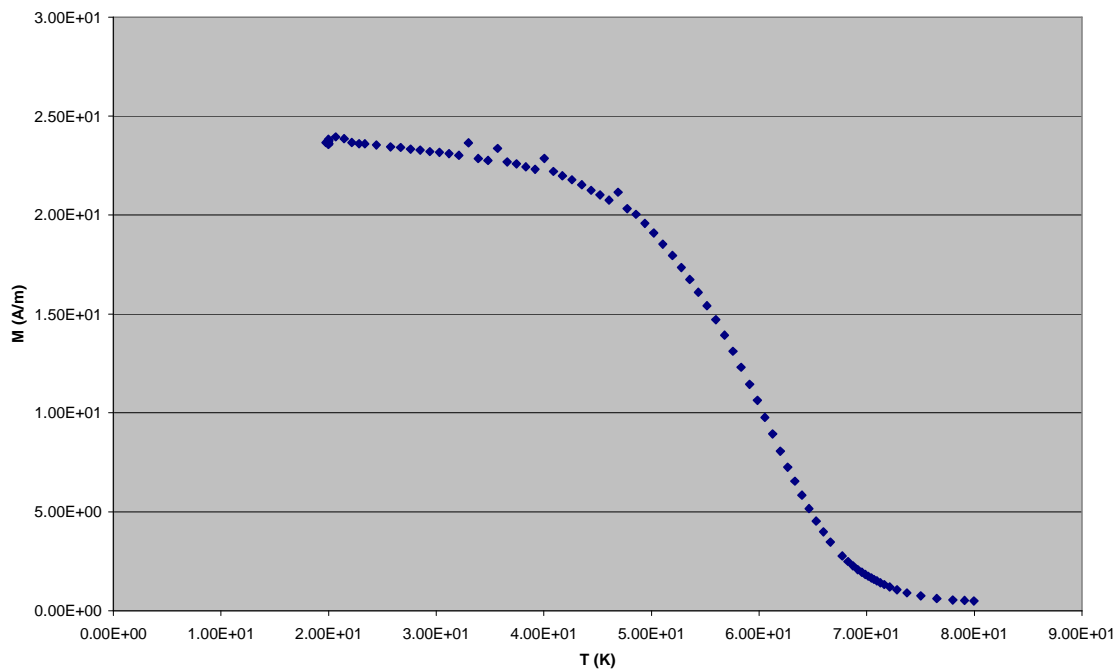
Figure 7-8 – Temperature vs. Magnetization for silver bound puck (data collected 19/06/2006)

A clear and repeatable transition is seen at about 60K in the above plot, with a significant change in the recorded magnetisation. A set of MH curves were also produced at various temperatures both above (60K) and below (15, 30K) the ferromagnetic transition. These are shown below:
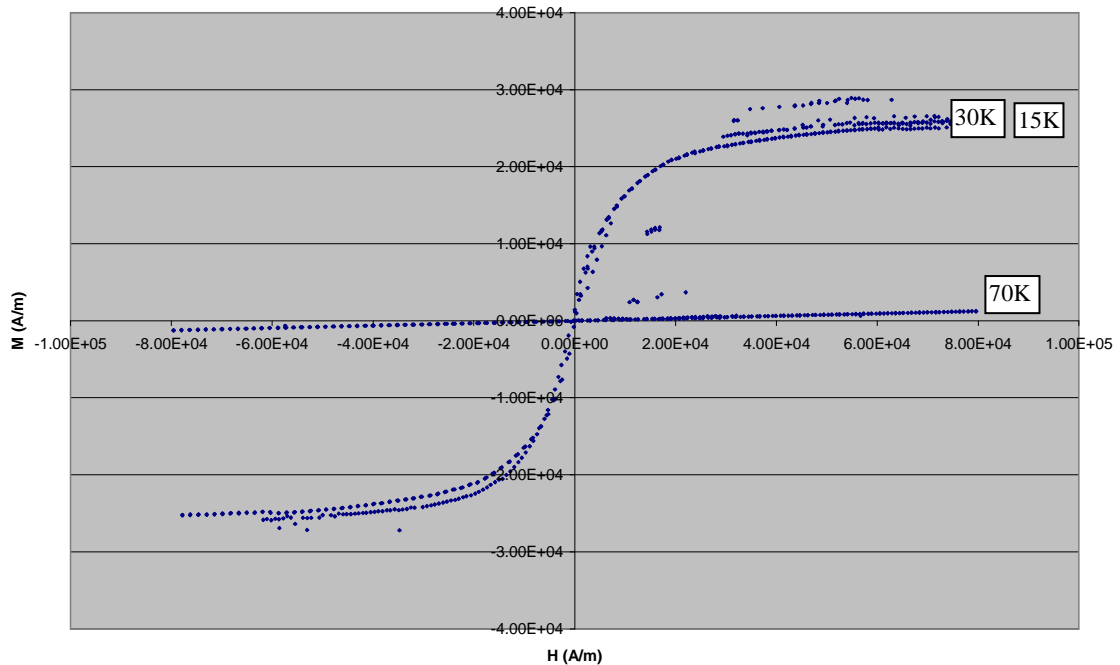
Figure 7-9 – MH curve for silver bound puck (data collected 19/06/2006)

The gradient of the linear section of the above plots can give us the relative permeability of the material (see page 36)

The plot @ **60K** gives a relative permeability of **~1**
The plot @ **30K** gives a relative permeability of **~3.5**

It will be seen that there is a little difference between the results obtained with the raw powder and those obtained with the puck, both giving a permeability change from ~1 to ~3.

7.2.4 Fine Powder SQUID results

It was noted earlier that the raw powder crumbled to an extremely fine, brown powder. Previously this powder had been ignored as an unwanted by-product whose size was so small that superparamagnetic behaviour was likely.

However, because the powder was so fine, once made up into a puck the packing factor was so high that VanDerValls forces could keep a puck of the material together. If this material did not exhibit superparamagnetic behaviour, then it could be extremely useful. To ascertain whether superparamagnetic behaviour was being displayed, a final set of SQUID measurements were taken, this time with a puck of the crumbled powder:

MH Loops
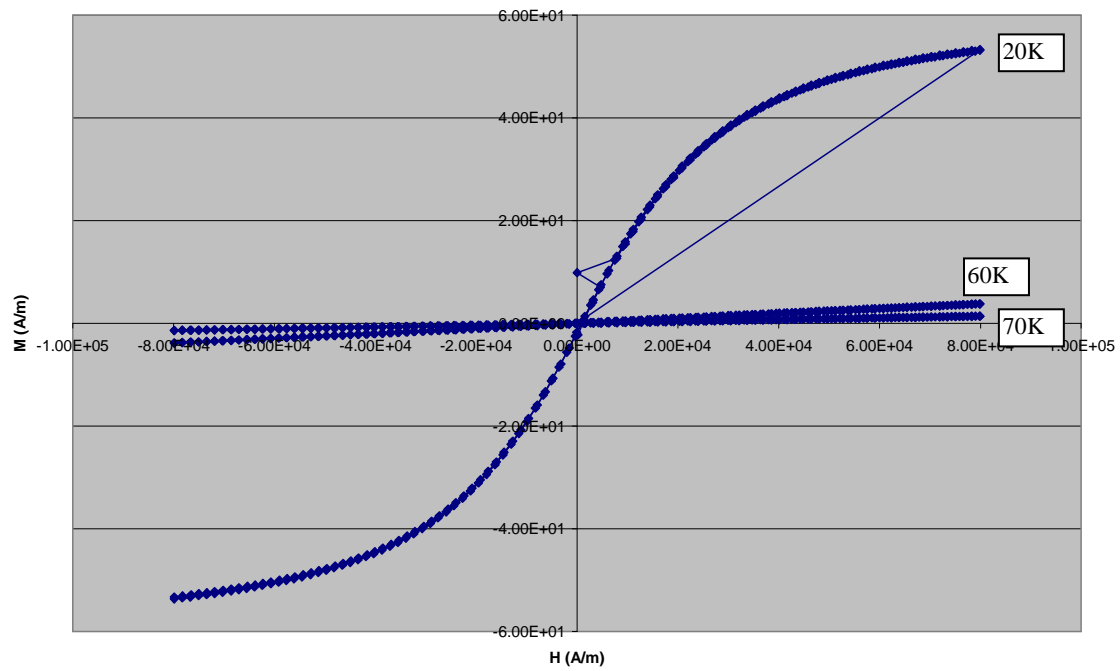
Figure 7-10 – Fine powder puck with no binder – data collected 01/08/2006

TM Plot
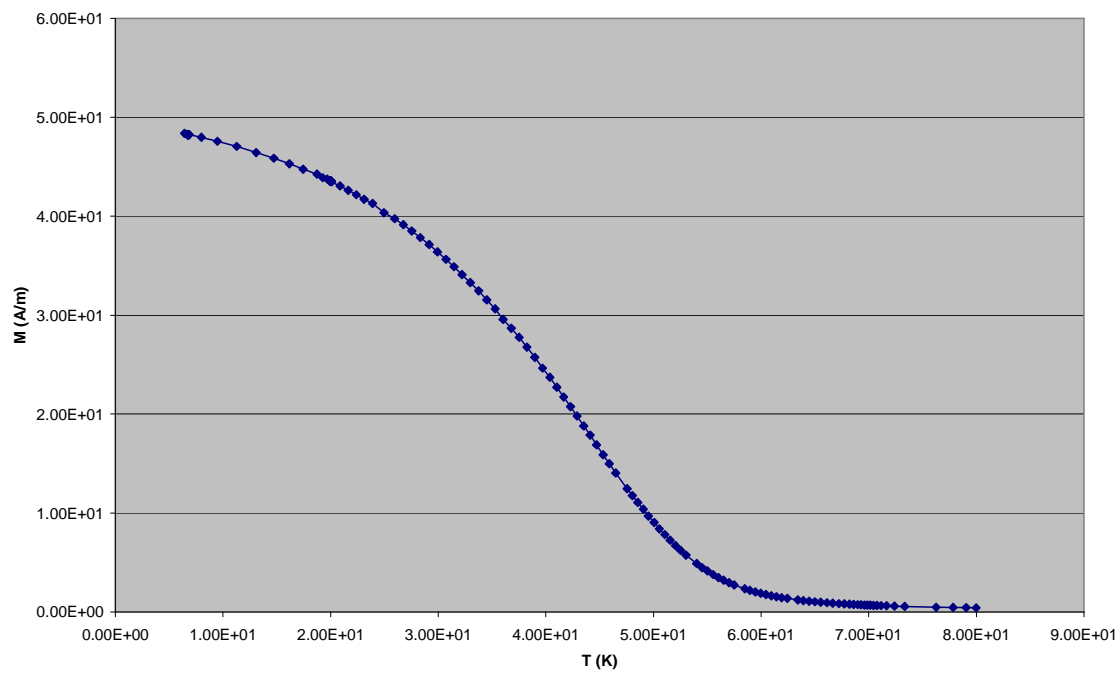
Figure 7-11 - Fine powder puck with no binder – data collected 01/08/2006

In the plots above for the fine powder it can be seen that, as predicted, superparamagnetic behaviour is evident. Although there is still a transition visible at ~60K, the magnitude of the magnetization is far less, with a maximum relative permeability of barely over 1. So while the fine powder has advantages in that it does not require a binder it is, unfortunately, no longer exhibiting the desired magnetic properties.

7.2.5 Microanalysis of Prussian blue analogue

It was suspected that the reason for the significantly lower values of relative permeability when compared to those predicted could be due to us not creating the material we thought we were creating, or at least not creating as much of it. To check this theory a microanalysis was carried out on the prepared powder. At the same time, having failed to achieve as high a change in permeability as predicted with our first analogue, another, similar analogue was prepared:

$$\text{C}_8\text{H}_2\text{0N}Ni^{II}[Cr^{III}(CN)_6]$$
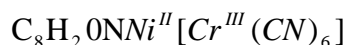
This was suggested by colleagues in the chemistry department, and it was hoped that this analogue would have a similar transition temperature to our previous candidate, but with a more pronounced change in relative permeability.

At the time of writing, the microanalysis had still not been completed (due to staff shortages over the summer period). However, it is thought likely that when they do return they will shed some light on the lower than expected permeabilities. Having said that, as will be seen later in this report, even the changes measured should be sufficient to test our theories.

7.2.6 Raw powder – second analogue

As with the previous sample, we corrected for demagnetization and packing factor when analysing our SQUID data. However, there was some uncertainty in calculating the density of the new analogue. The chemical equation is:

$$\text{C}_8\text{H}_2\text{0N}Ni^{II}[Cr^{III}(CN)_6]$$
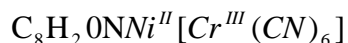
Our density for the previous analogue was calculated using the assumption that the cell size of $NaMn[Cr(CN)_6]$ was similar to that of our analogue, $Ni_{1.5}^{II}[Cr^{III}(CN)_6]$. Using this method yields the following results:

The molecular mass of our the new analogue was 304.85g/mol

1 mole contains 6.02×10^{23} molecules (Avogadro's constant)

Thus one unit cell weighs:

$$\left(\frac{4}{6.02\times10^{23}}\right)\times304.85 = 2.026\times10^{-21}\,g$$

Giving a density of:

$$\frac{2.026\times10^{-21}\,g}{1.2653\times10^{-21}\,cm^3} = 1.60\,g/cm^3 = 16000\,Kg/m^3$$

However, our new analogue, with the large $(C_8H_2ON)^+$ ion, far larger than the sodium or nickel ions, is likely to invalidate this method, as it will significantly alter the cell size, meaning that the above density value would be an overestimate.

Thus in this case the figure for packing factor was obtained by assuming reasonably spherical crystals (the crystals were far more regular than our first analogue), and using the fact that a unit sphere in a unit cube occupies 53% of the volume. Future work is needed to calculate the density, experimentally, of the materials produced, however there will be significant problems with measuring the density of the powder. Although water insoluble, we can not create enough easily to measure displacement, so another method must be found.

A sample of this new material was produced, in powder form, and tested in the SQUID. The results are shown below:

MH Loops:

MH Loop
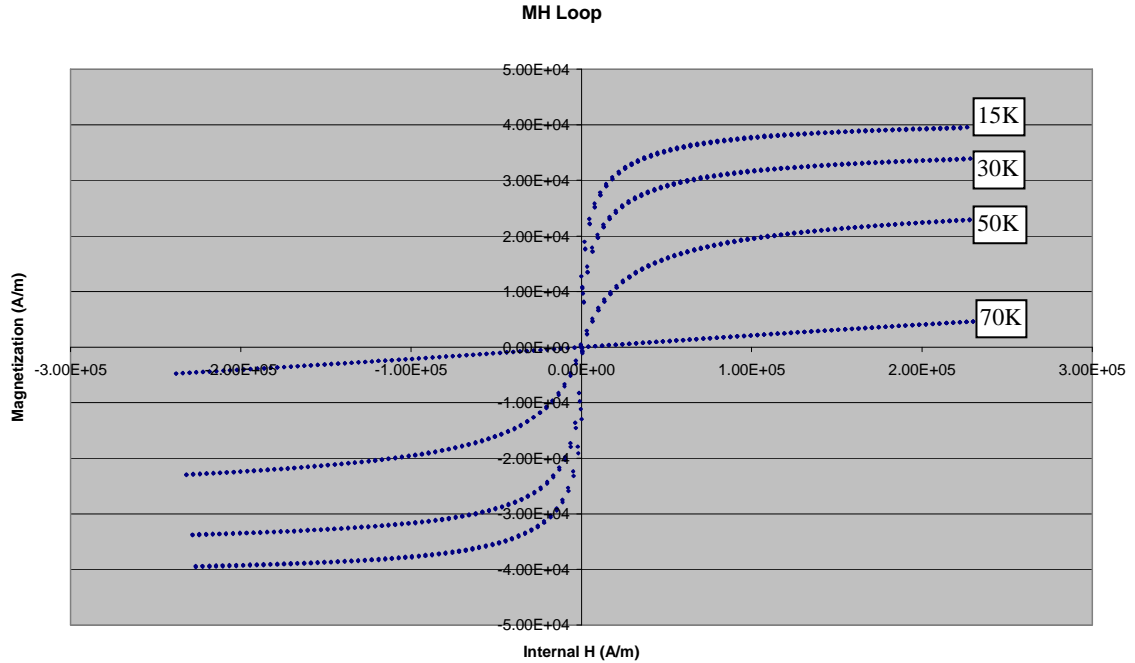
Figure 7-12 – Second analogue ($C_8H_2 0NNi^{II}[Cr^{III}(CN)_6]$) MH plot (data collected 07/08/06)

It can be seen that the loops cross the y axis. This can be attributed to the skew in the graph due to the demagnetization factor:

$$H_{Internal} = H_{Applied} - NM$$

If the value of N is not exactly correct, then the graph will be skewed to the wrong extent. Our demagnetization factor was calculated assuming an ellipsoid sample. Our SQUID sample was a cylinder of diameter and length 5mm. Modelling this as a sphere gives a demagnetization factor of a third. However, any errors this introduced are likely to be small.

From the analysis of our earlier plots we know that the relative permeability is given by:

$$u_r = 1 + \frac{M}{H}$$

Erring on the side of caution for the reasons outlined above still gives us the following perm abilities:

@ 30K $u_r \approx 6$

@70K $u_r \approx 1$

It can be seen that the measured permeability is significantly higher than with the first material studied (roughly twice as large), though still far below the 52 predicted initially. However, it should be noted that due to the density problems outlined above there is a significant room for error in this value which needs to be addressed through collaboration with the chemistry department at a future date. There was insufficient time during the year to make up pucks of the second material, but there is no reason to suppose the results would differ greatly, since the binder itself is non-magnetic. However, erring on the side of caution the rest of this thesis will deal only with the first analogue whose properties we are more certain of.

TM Plot:

TvsM
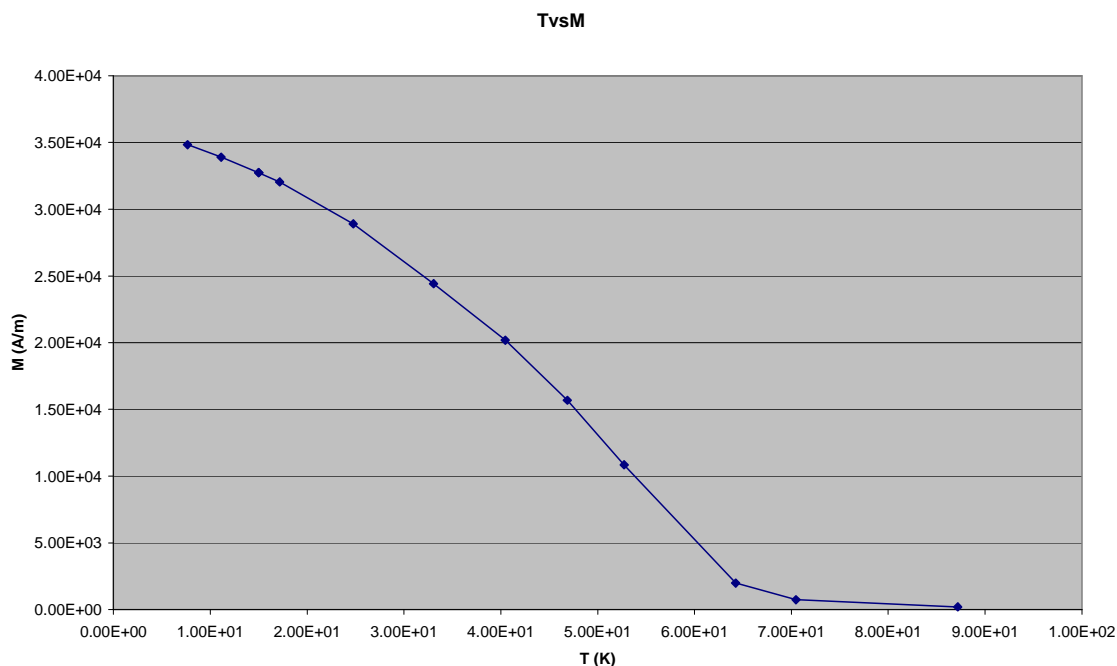
Figure 7-13 - Second analogue ($C_8H_2 0NNi^{II}[Cr^{III}(CN)_6]$) TM plot (data collected 07/08/06)

8 Design of rig to test theory

The simulations presented earlier illustrated that a TAS should function. Realising an experimental setup which would replicate this setup was the next step. Our simulation depicted a cylindrical sample of variable permeability material, with an area of high permeability moving in from the outer edge.

To replicate this we need a cylindrical sample of material, with a toroidal ring of high temperature that travels into the centre from the outer edge. There were two distinct approaches that were examined to produce this effect:

- Forced heating
    - The other option investigated was forced heating. If we have a low conductivity material, then we can heat it locally without affecting the surrounding area. So if, for example, if an array of transistors could be produced, then we would be able to switch the permeability of the sample as we would switch a pixel (heat dissipated in the transistor driving the material over its transition)

- Thermal wave
    - If the outer edge of the sample is heated with a pulse, then that heat pulse should travel inwards as a toroidal ring towards the centre. Achieving this depends on obtaining favourable thermal properties such that we can produce a slow moving leading edge rather than the entire block heating up simultaneously.

Both of these approaches require us to know the thermal properties of our material. During initial work we were still working with the puck held together with silver binder (the fine powder had not yet been examined), and it is to this bound puck that we will refer in the following sections.

To date we have not characterised the thermal properties either of the raw powder, or of our silver puck. However, discussions with colleagues in the chemistry department suggested that the powder would be a thermal insulator. Based upon that surmise, we were able to estimate the thermal properties of our puck:

If we assume that our puck has a packing factor around 90%, and assume that the Prussian blue powder itself has:

thermal conductivity << silver, and specific heat >> silver

then we can take the thermal properties of the puck to be 10% those of silver

@25 degrees C:

Specific heat capacity = 10* 232	=	**2320 J/Kg K**
Thermal conductivity = 0.1*418	=	**41.8W/mK**

8.1 Forced Heating

A forced heating approach would appear to be the most flexible. An array of transistors would enable any pattern of permeability to be produced. However, it would not be a trivial task to produce such an array, and would certainly fall outside the expertise of this group. In the interim however, a simulation was run based upon concentric heating "elements". These could be PCB tracks through which current was passed, and which would then dissipate energy to the Prussian blue, raising its temperature. While less flexible than a full array, it would also be far simpler to produce.

8.2 Thermal Wave

The alternative to forced heating was to simply heat up the circumference of our puck with a heat pulse, causing a thermal wave to propagate towards the centre. This method is far simpler than the forced wave above, but it is more dependant on favourable thermal properties of the material.

To test whether our material was likely to have the necessary thermal properties, a simple model was constructed. It showed a block of our material connected to a cold head. The thermal path from the sample to the cold head was interrupted by a heat source, enabling us to heat up the sample via its outer edges.

8.2.1 Thermal Model
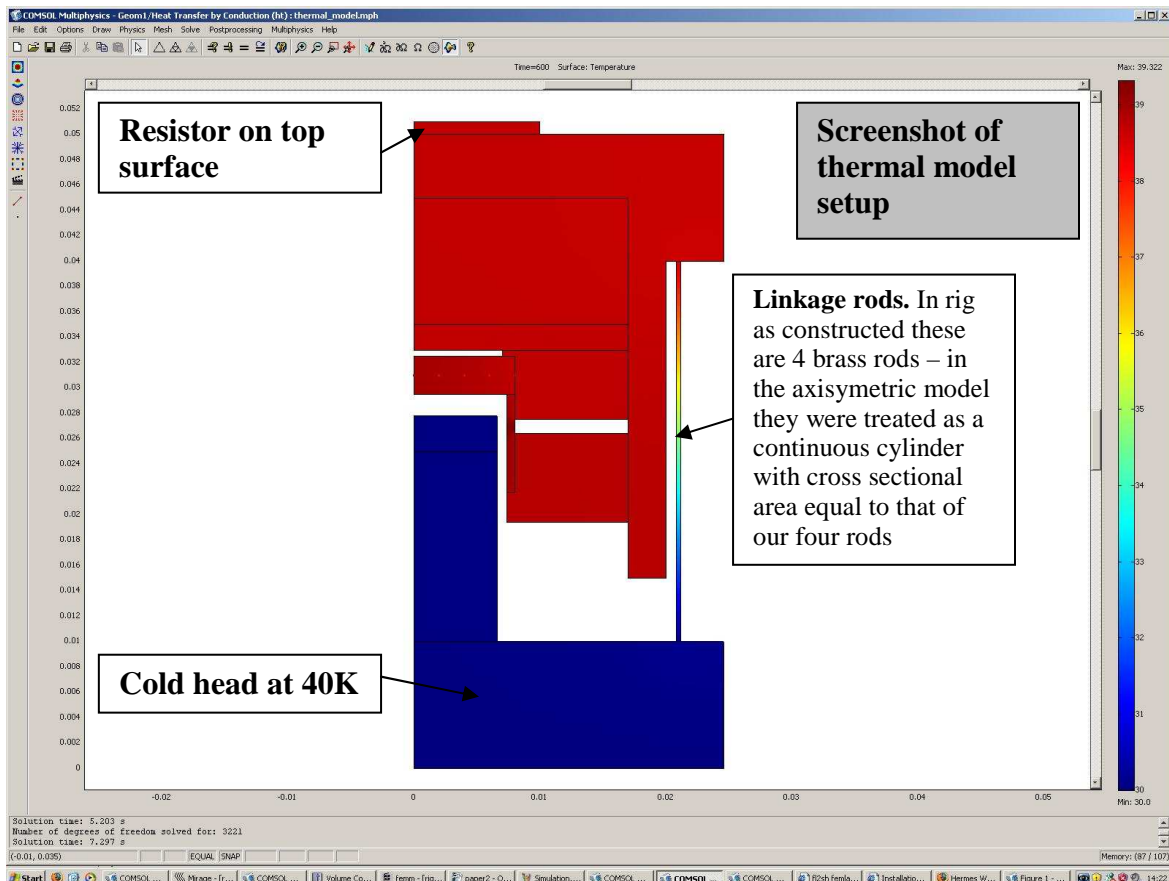
Figure 8-1 – Screenshot of thermal model. The cold head is held at 40K while a step heat input is applied to the resistor on the topmost surface and then removed.

The model was set up with a 25W heat input to the block on the top of the rig, shown above. This pulse was modelled as a step that turned off after 300 seconds. The base of the rig was modelled as being tied to 30K – our cold head temperature.

A series of plots were produced showing the temperature at various points across the Prussian blue puck with respect to time:
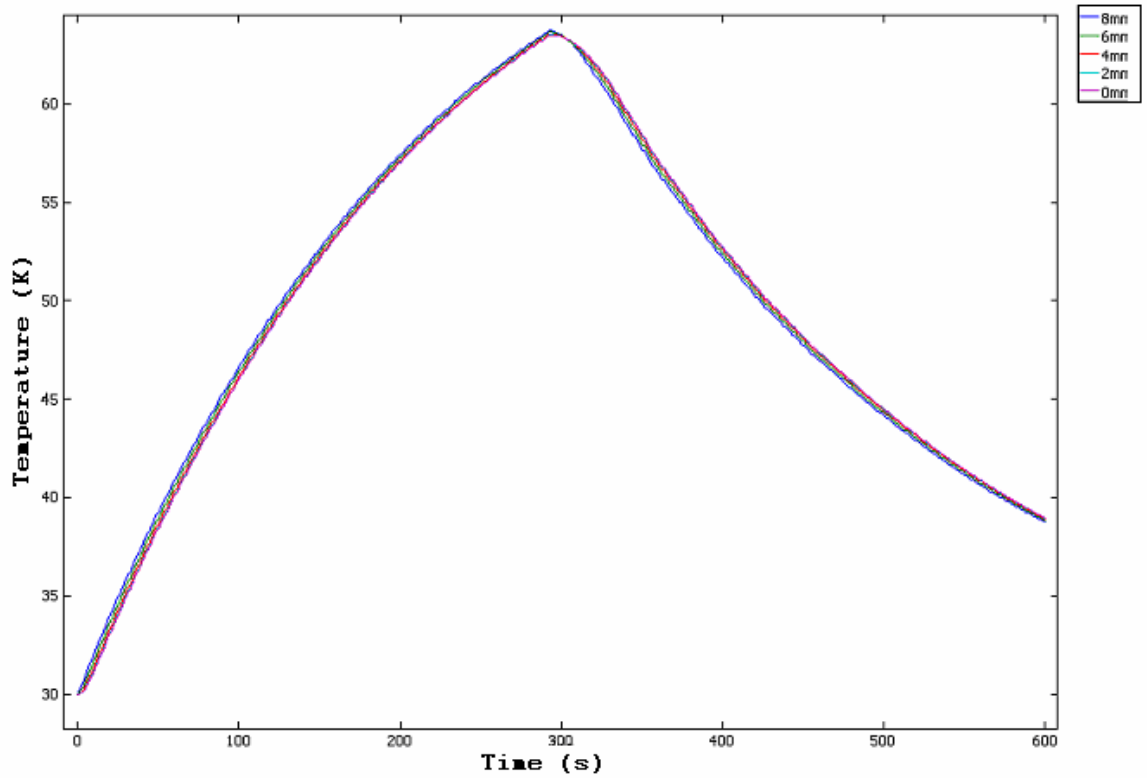
Figure 8-2 – Output from thermal model for 25W input

This plot shows the puck first heating up, then cooling down over a period of 10 minutes. The 5 lines plotted represent five points in the puck, each separated by 2mm, from the outer edge to the centre. While the lines lie very close to each other, there is a definite delay from one to the next. This can clearly be seen on the following, zoomed in plot:

53
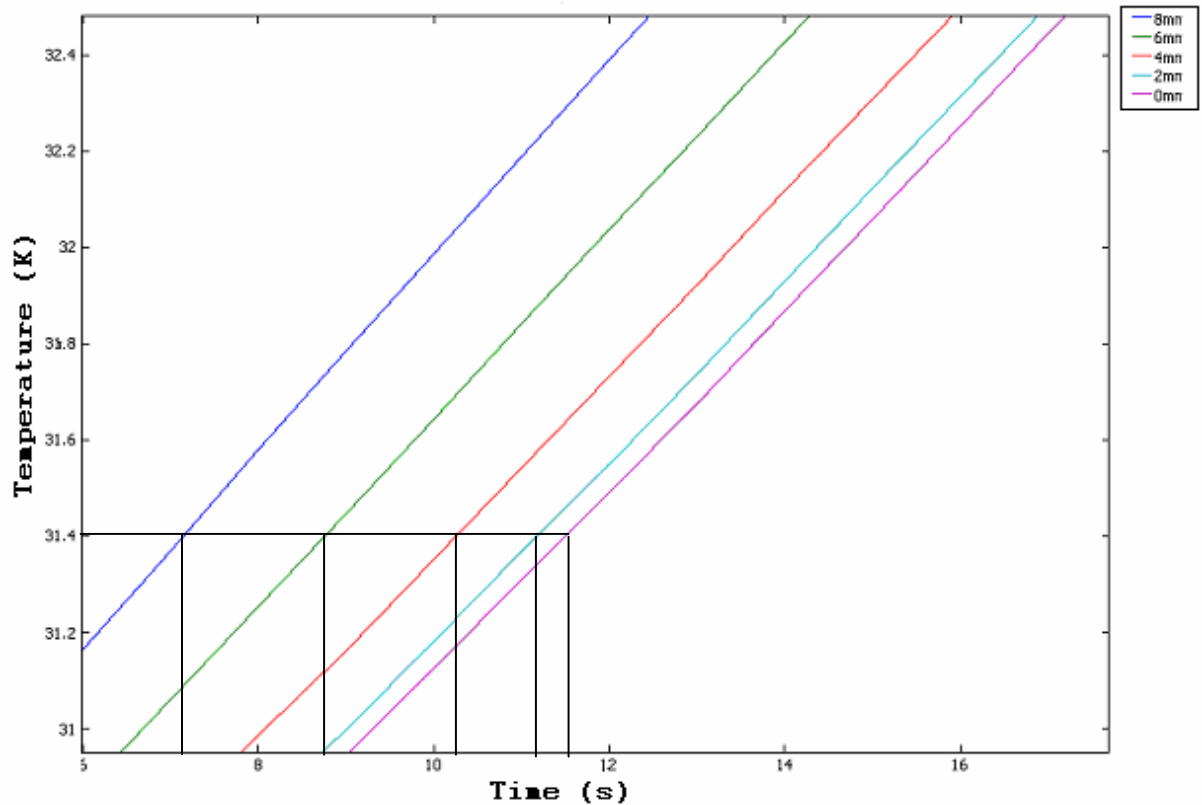
Figure 8-3 – Output from thermal model, zoomed in to show wave progression

In the above plot each of the lines from left to right represents the temperature at a point further within the material (see key). The black vertical and horizontal lines show the time separation between different temperatures within the material as the wave travels inwards.

This plot clearly shows a thermal front moving through the material. Again, each line on the above graph represents a 2mm separation, with the outer edge of the puck represented by the left hand line, and the centre of the puck by the right hand line. It can be seen that the pulse takes approximately 4 seconds to travel from the outer edge to the centre, with this speed increasing as the pulse penetrates further. Of course this result will depend on the exact thermal properties of the material, but it does show that such an approach is viable.

8.2.2 Magnetic Model

A series of magnetic models were also produced. We needed to show that, having produced a thermal wave, we could turn this into a magnetic wave due to the ferromagnetic transition of our Prussian blue analogue. In this simulation, a change in relative permeability from 1 to 3 was used. This agrees well with the change observed from our SQUID measurements of the two Prussian blue analogues. As mentioned, there was some uncertainty as to the density, and thus the precise volume present, of our

54

second analogue. However, any error would serve to increase, not decrease the change in permeability above that of our first sample.

In designing the magnetic simulation, it was realised there was a conflict in design needs for our rig. On the one hand a high conductivity, low specific heat material such as copper was needed to facilitate our thermal pulses. However, on the other hand it was necessary for the dimensions of our Prussian blue puck to be significant with respect to the size of the magnetic circuit (which will thus give a bigger effect for a given change in the Prussian Blue's magnetic properties).

This would entail constructing the rig from soft iron, which has a high permeability, but a far lower thermal conductivity.

Our first simulation was designed assuming an all copper rig, but with the superconductor mounted on an aluminium pedestal, and the various spacers within the copper block also constructed from Aluminium (to prevent binding between similar metals) (see *Figure 8-7*)

The simulation modelled a heat pulse being applied to the outer edge of our puck, an then travelling towards the centre. This was followed by the sample cooling down, again from the outer edge (see *Figure 1-5*, page 5)

To do this, the puck was modelled as 8 strips of material that we could set to either hot (low permeability) or cold (high permeability) as the pulse advanced:

Spacer to hold hall probes

The simulation was run multiple times, each time changing the parameters of the strips of Prussian blue to model an advancing thermal wave

Pedestal on which superconductor sits
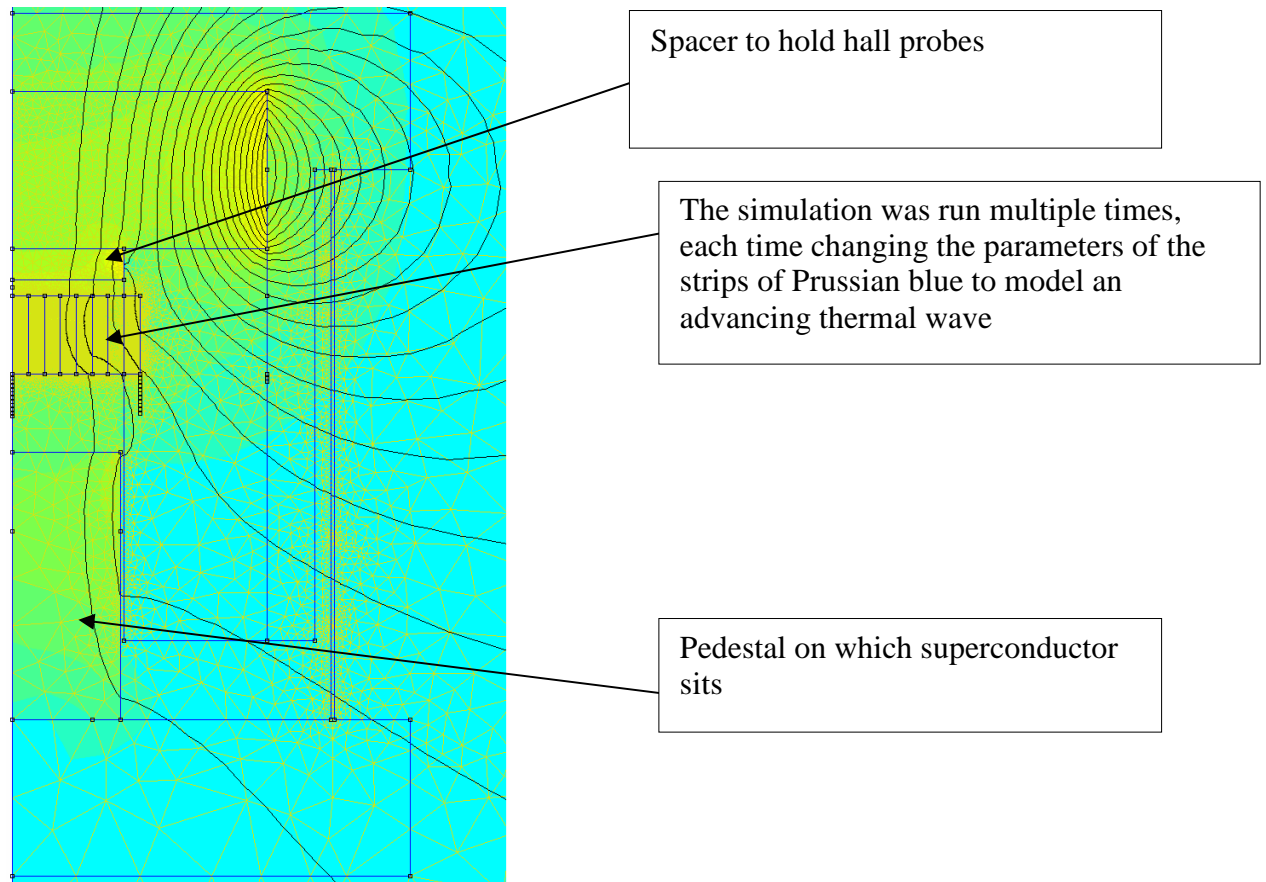
Figure 8-4 – Magnetic model, showing finite element mesh

This gave the following plot for our magnetic wave 0.8mm bellow the bottom surface of our
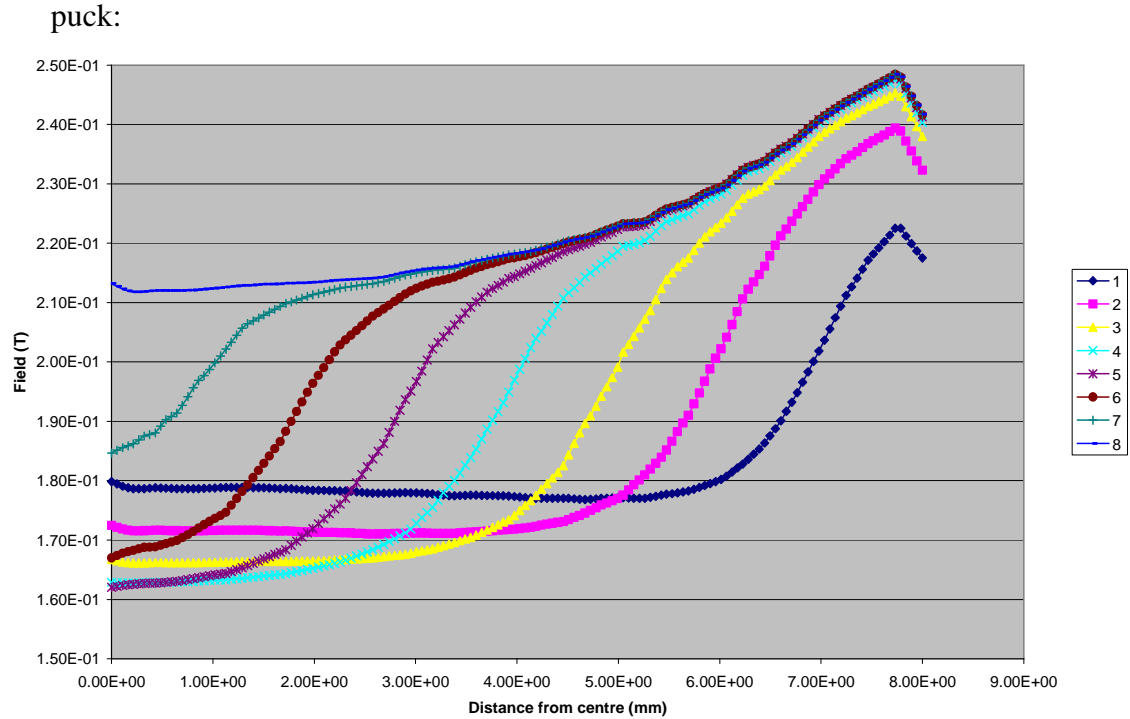
puck:

Figure 8-5 – magnetic field strength 0.8mm below the surface of the puck for heating (top) and cooling (bottom) for a change in relative permeability of 1 to 3

During both heating and cooling, there is a peak of at least 30mT visible. While this might be sufficient,   the simulation was then modified such that the pedestal on which the superconductor sits was made from soft iron, as was the spacer above the Prussian blue, between it and the magnet. This has the advantage of introducing a large amount of soft iron into the circuit, without interfering with the thermal circuit through the copper, and gave the following plot, again 0.8mm below the Prussian blue surface:
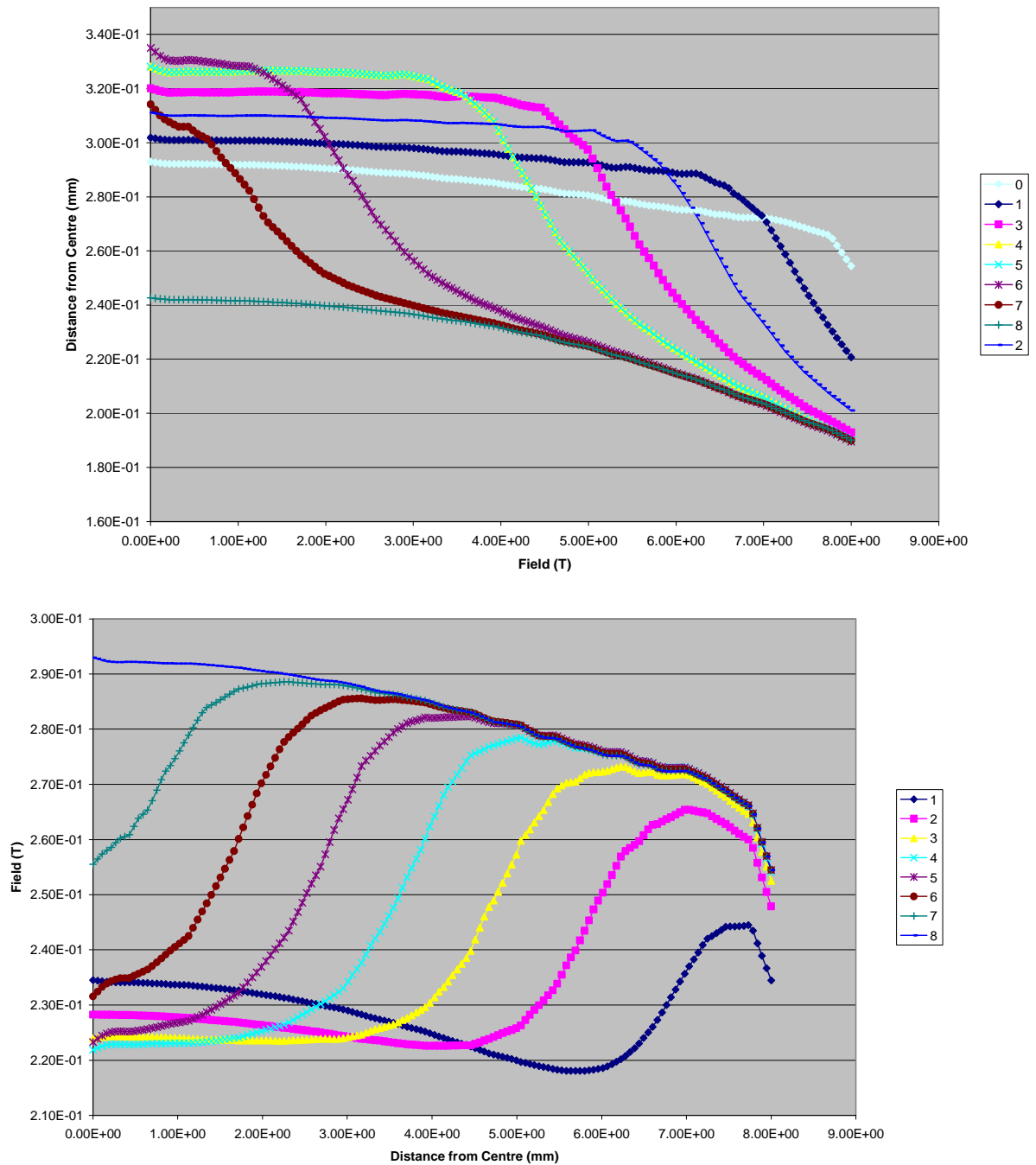
Figure 8-6 – Magnetic model 0.8mm below Prussian blue surface, but with an iron pedestal for the superconductor

There is a noticeable change between the two models. In the case of the iron pedestal, the magnitude of the field measured is increased. However, the sharpness of the magnetic wave-front is reduced, meaning there may be no overall advantage to using the iron.

It is likely the reason for this is lies in the fact that the permeability of our Prussian Blue is << that of the iron. In the case of the Al pedestal, a change in permeability of 1->3 is more significant than when we have an iron rod, with a very high relative permeability, right next to our Prussian Blue sample. Although the field measured will be higher in the second case due to the flex concentration caused by the iron, the change due to our Prussian blue will be less pronounced.

However, there is still an issue with the penetration depth of the wave. The above plots were taken at a depth of 0.8mm below the puck – by 2.5mm below, any effect has nearly vanished. This penetration depth could be increased by improving the magnetic circuit in a future design (making the Prussian blue a larger proportion of the total circuit) However in this instance it can be seen therefore that the superconductor and the Prussian blue must be in very close contact if the wave is to penetrate.

8.3 Constructing the experiment

Based upon the above simulations, it was decided to attempt a thermal wave, rather than a forced actuation. While the former would be more flexible, it would also be significantly more complex to construct, and for an initial test the simplicity of a thermal wave was an advantage.
The applied magnetic field would be provided by a high grade NdFeB permanent magnet, below which would be hall probes, then the Prussian blue puck, and finally the superconductor.

The rig was built to match the simulated structure shown above, and is shown diagrammatically below:

Thermocouple 1

Heater

NdFeB Magnet

Hall probes

Prussian blue/silver binder puck

YBCO high temperature superconductor

Cold Head

Washer to protect hall probes

Thermocouple 2

Washer to hold sample

Brass rods enable top section to slide up and down – very tight fit to ensure a good fit and good thermal path

Aluminium plug screws into base and holds sample (and everything above it) in

Figure 8-7 – Initial setup of experimental rig (not to scale). Details changed from experiment to experiment, and are documented where applicable.

Initially, it was thought that there could be a problem with the experimental setup. The top section of the rig is constructed from copper, and joined to the bottom section by 4 tight fitting brass rods, each 1/8" in diameter. If the thermal expansion coefficients were sufficiently different for brass and copper, and the right way around (so the joints loosen rather than tighten with falling temperature) then it is possible they could lose contact, and thus interrupt the thermal path from top to bottom. To check this figures were obtained for the thermal expansion coefficient of both copper and brass at cryogenic temperatures:

Fig.3.14. Relative linear thermal expansion coefficient of (1) Invar (upper), Pyrex (lower), (2) W, (3) non-alloyed steel, (4) Ni, (5) $Cu_{0.7}Ni_{0.3}$, (6) stainless steel, (7) Cu, (8) German silver, (9) brass, (10) Al, (11) soft solder, (12) In, (13) Vespel SP22, (14) Hg, (15) ice, (16) Araldite, (17) Stycast 1266, (18) PMMA, (19) Nylon, (20) Teflon [3.44]. Some further data are: Pt similar to (3); Ag between (9) and (10); Stycast 2850 GT slightly larger than (10). The relative change of length between 300 and 4 K is $10^3 \Delta\ell/\ell = 11.5, 4.2, 6.3$ and 5.7 for Stycast 1266, Stycast 2850 GT, Vespel SP-22 and solders, respectively [3.43–45].

Figure 8-8 - "Matter and Methods at Low Temperature"[27]

It can be seen that although the coefficients are ordered such that a decrease in temperature would lead to a looser fit, the values are so similar that the effects are likely to be negligible at the temperatures we will be working at.

---

[27] Frank Pobell, 2002 Springer
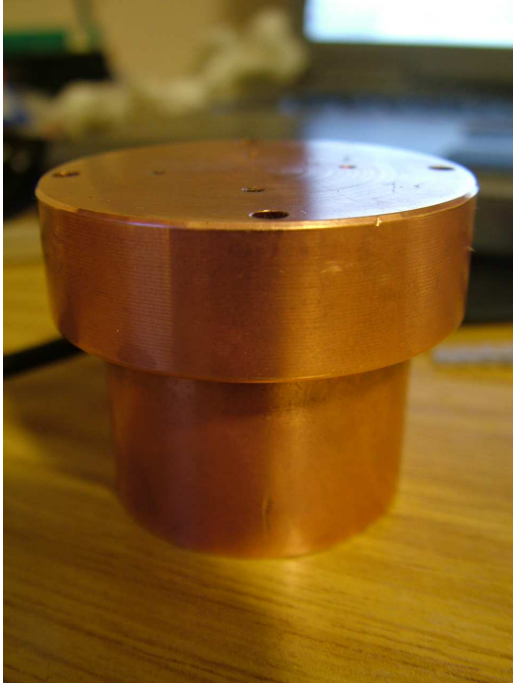
Figure 8-9 – Top section of the copper rig

One issue that needed addressing was how far from the superconductor the puck could be. It needed to be separate so as not to provide a conductive path, but any magnetic wave produced by the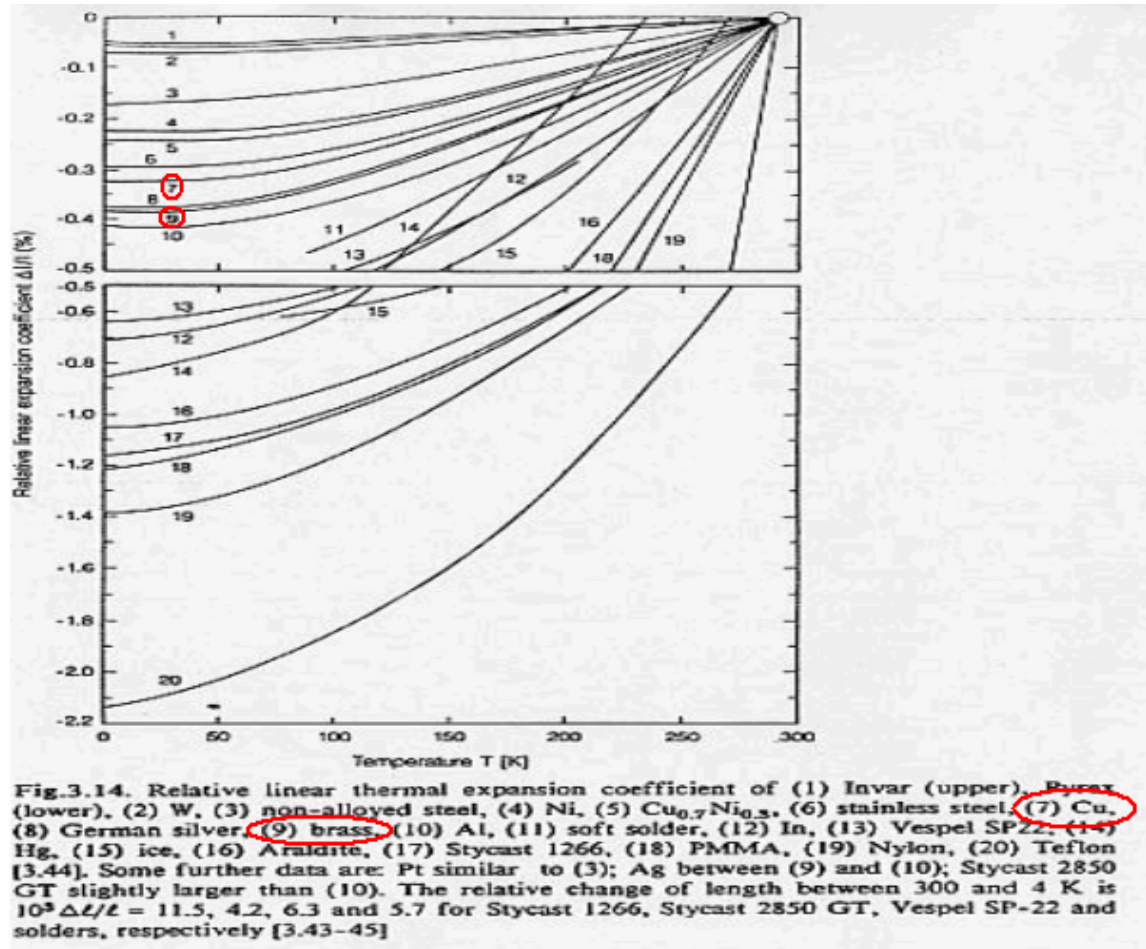 puck was likely to be very short range (see *Figure 8-5*, page 57). To test this, a simulation was put together to model how the magnetic properties changed with distance from the puck, as the puck crossed its magnetic transition.

The rig was built from copper for its high thermal conductivity. However, being non-ferromagnetic it also meant that the majority of the magnetic path of our permanent magnet was through air. There was a concern therefore that the changing properties of the puck, whose dimensions were << than that of the circuit, would have a small impact on field distribution. The earlier magnetic simulations seemed to suggest however that a wave would be visible, and furthermore that making the pedestal for the superconductor from soft iron would increase the amplitude significantly.

The structure itself was encased in an evacuated cryocooler, such that the only heat transfer could be either via conduction or radiation. The cooler was a closed circuit liquid He system, capable of reaching temperatures down to 4.2K under ideal conditions[28].

The power resistor on the top surface enabled us to heat up the edges of the sample puck. The superconductor itself is in direct contact with the cold head, with a small gap

---

[28]   Our conditions were not ideal – the compressor for the helium was replaced due to old age. As a result, the cooling capacity of the cooler fell considerably.

between its top surface and the puck, to prevent it being driven normal by the thermal wave.

Two thermocouples were attached to the outer surface of the device, on the top surface near the heater, and on the outer surface, level with the edge of our puck. These were fed through compensated cables out of the cooler to a PC. The temperature of the cooler itself was monitored by a silicon diode whose output was fed back to a PID controller unit.
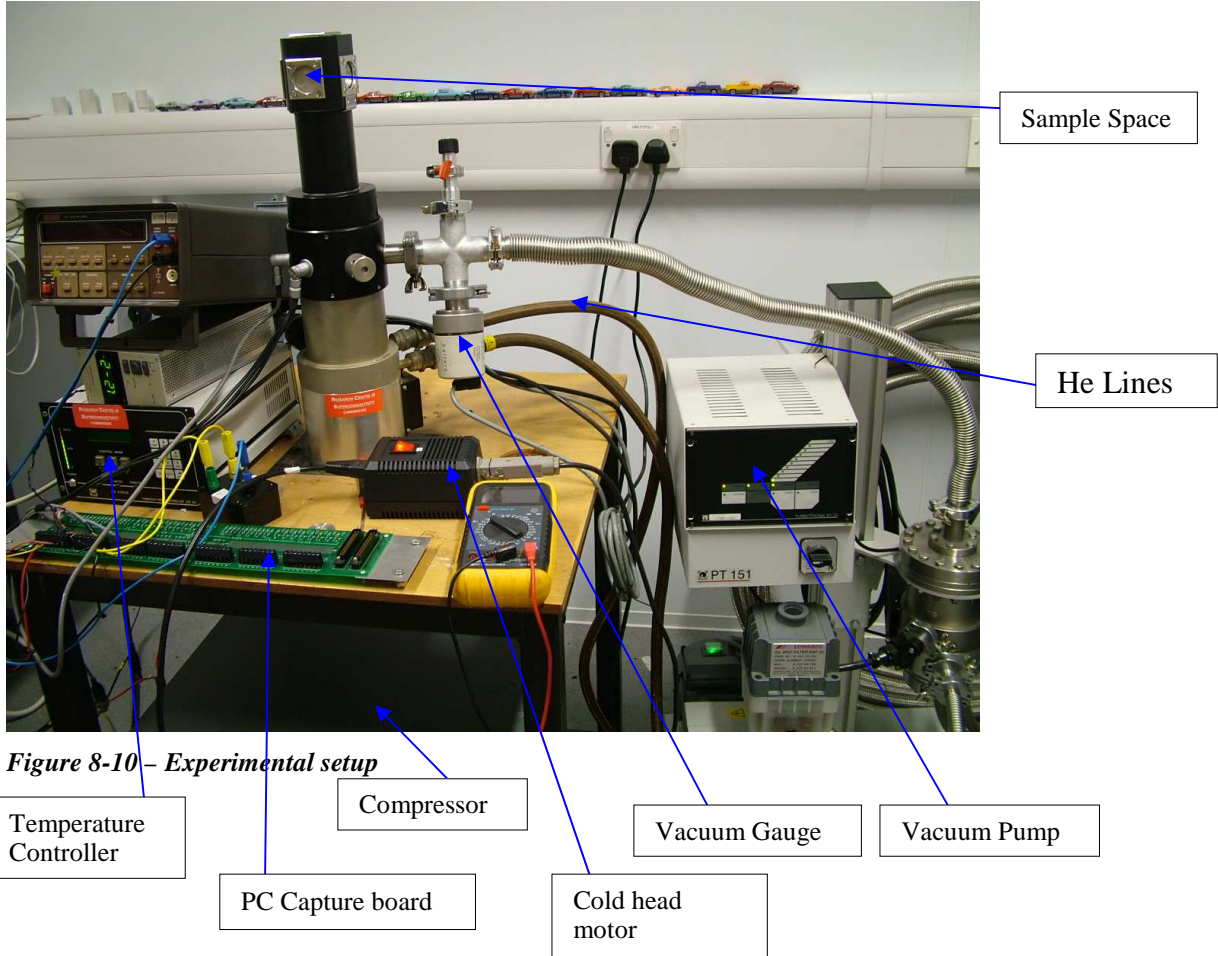
Figure 8-10 – Experimental setup

Two high sensitivity, high linearity hall probes[29] were fitted inside the experimental rig in between the permanent magnet and the top of the Prussian blue, with which it was hoped to measure any magnetic wave produced. These were wired to a 50mA current source, with the voltage leads running to a PC.

8.3.1 Radiation losses

We have assumed in designing our experiment that all heat transfer is by direct conduction, and that there is negligible radiation. If this were not the case, then our thermal path could be shorted out (for instance radiating from the superconductor to the base of the puck could tie it permanently to the cold head temperature)

---

29   LHP-NP from "Arepoc" : http://www.arepoc.sk/default_soubory/LHP_N.htm

To ensure that this was not the case, we set up a finite element model to determine the steady state temperature with the cold head at 40K. Radiation losses appeared tiny:

Figure 8-11 – Second thermal model showing negligible radiation losses

The key on the right hand side shows that the radiation to ambient (280K) is negligible, with the entire unit staying at a uniform 40K, even without a radiation shield.

We will be able to check this once the experiment is running. Conduction heat transfer is governed by the following equation:

$$Q = \frac{kA(T_o - T)}{L}$$

Radiation by this:

$$Q = A\varepsilon\sigma(T_o - T)^4$$

It can be seen that while conduction losses are directly proportional to the temperature difference, radiation losses are proportional to the 4th power of the difference. Thus if our thermocouples show a purely linear change in temperature with time, we know radiation losses are small.

9 Introduction to the cryocooler

9.1 Refrigeration Cycle

The cryocooler at is simplest is a device that pumps liquid helium (boiling point 4.2K) through an cold head located in an enclosed, evacuated space. The actual temperature of the cold head is determined by a heater mounted on its top surface, in theory allowing any temperature between 4.2K (in fact minimum rated temperature is 10K) upwards to be obtained. As the helium passes through the cold head, if that cold head is above 4.2K the helium boils, cooling the cold head. The gaseous helium is then returned to the compressor, the heat extracted (via a water cooling system) and the gas condensed ready for another pass.

Our cooler is slightly more complicated. A valve at the base of the cold head opens and closes valves in the helium lines to make use of the Gifford-McMahon cycle:

(In the following diagrams, the regenerator is thermally linked to the cold-head)
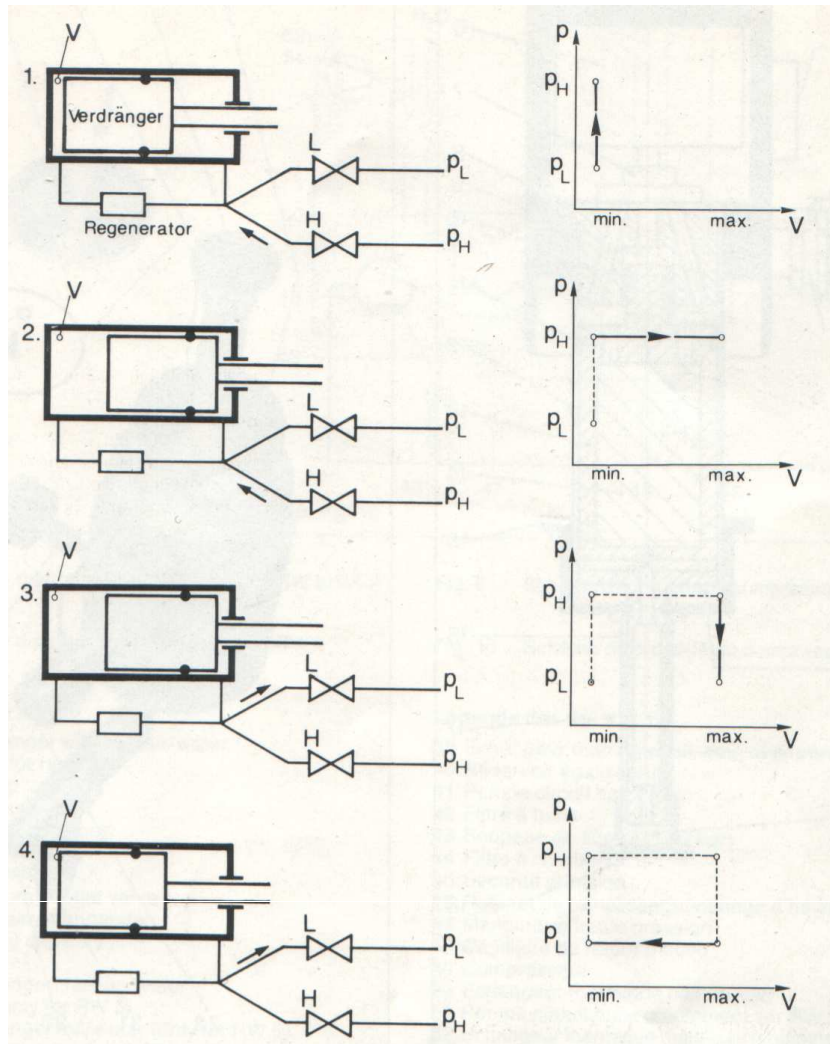
Figure 9-1 – Gifford-McMahon refrigeration cycle explained

The PV product gives us the amount of energy stored in the gas:

P   V   J

$$\frac{N}{m^2} \times m^3 = Nm$$

Thus ideally the total heat extracted from the cold head in one cycle is given by:

$$Q = (V_{Max} - V_{Min})(p_H - p_L)$$

The cooling power of the cold head obviously depends on the flow rate of the helium - how many times the cycle repeats per second, and this is a function of the compressor unit used.

9.2 Two stage Cold head

Our system consists of two cold heads, a high power and a low power one. The high power cold head will sit at around 40K. It is strongly tied to this temperature due to the high power of the head. The smaller secondary cold head has less power, and so the temperature controller can vary its temperature as needed. It has the ability to drop the temperature down as far as (nominally) 10K.
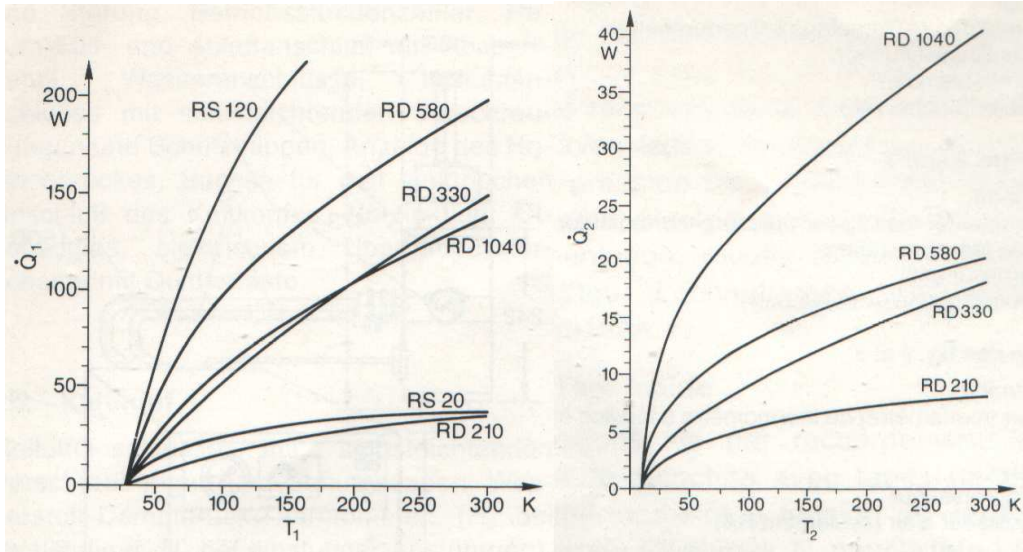
Figure 9-2 – Power vs. Temp for first stage (left) and second stage (right)

The above figures show the cooling power of the primary and secondary stages respectively (our unit is an RS210)

10 Calibrating the system

Having produced the final system, we set about testing the rig. The first task was to check the output from our sensors at room temperature and pressure.

10.1 Thermocouples

It was discovered by Thomas Johann Seebeck in 1821 that any metal will produce a voltage when a temperature gradient exists across its length. The relationship is given by:

$$V = \sigma_s \Delta T$$

Where σ_s is the Seebeck coefficient for the material. If we create a general thermocouple circuit:
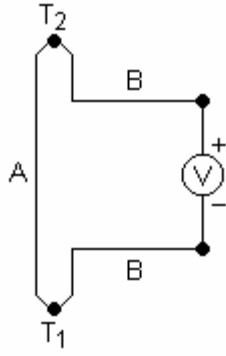
Figure 10-1 – Basic thermocouple circuit

Where material A has Seebeck coefficient σ_A and material B has coefficient σ_B
The voltage measured at the terminals will be:

$$V = \int_{Tj}^{T1} \sigma_B(T)dT + \int_{T1}^{T2} \sigma_A(T)dT + \int_{T2}^{Tj} \sigma_B(T)dT$$

$$V = \int_{T2}^{Tj} \sigma_B(T)dT + \int_{Tj}^{T1} \sigma_B(T)dT + \int_{T1}^{T2} \sigma_A(T)dT$$

$$= \int_{T2}^{T1} \sigma_B(T)dT + \int_{T1}^{T2} \sigma_A(T)dT$$

$$= \int_{T2}^{T1} \sigma_B(T)dT - \int_{T2}^{T1} \sigma_A(T)dT$$

$$= \int_{T2}^{T1} (\sigma_B(T) - \sigma_A(T))dT$$

So if we have two metals with different Seebeck coefficients, then we will develop a voltage across the output terminals that is proportional to the temperature difference between our reference and our measurement junction. If we know the temperature of the reference, we can then calculate the measurement junction.

In our setup, the thermocouples used were both T type (copper + constantan) to give readings down to -270 ^{0}C. The two thermocouples were wired as shown below:
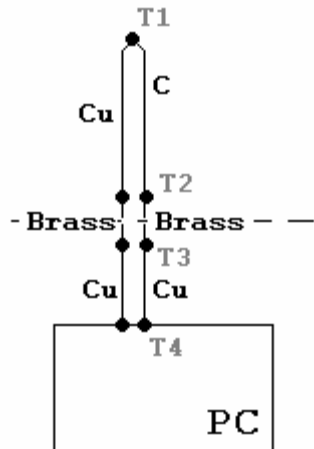
Figure 10-2 – Our thermocouple circuit

T1 is our measurement junction
T2 is our reference junction, at the inner junction of our brass connector
T3 is the temperature on the outer junction of the brass connector
T4 is the temperature measured by our capture card

To make a temperature measurement of T1, we have to make the following assumptions:

- Brass is an alloy of copper, and as such has an almost identical Seebeck coefficient
- T4=T3=T2

In that case our wiring simplifies to:
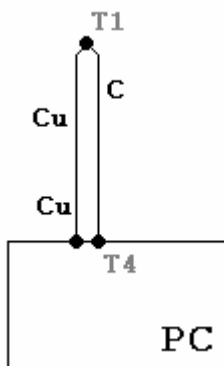
Figure 10-3 – Our thermocouple circuit, simplified

And the temperature can be read by the PC as:

$$V = \int_{T4}^{T1} (\sigma_{Cu}(T) - \sigma_C(T))dT$$

Standard lookup tables exist which relate the measured thermocouple voltage to the temperature at the measurement junction[30]. However, they are tabulated with respect to a reference junction (T4) at zero degrees Celsius. A correction must therefore be made for our non-zero reference temperature. This simply involves adding the voltage that a thermocouple would register at the reference temperature and a zero reference to the measured voltage.

10.1.1   Testing thermocouples

The first tests were carried out at room temperature and pressure using an ice bath (273K) and a vat of liquid nitrogen (77K) respectively. In both cases the calculated temperature was correct.

The next stage was to pump the system down and cool it, comparing the thermocouple readings to those from the temperature controller's silicon diode – again the match was good.

10.2 Hall Probes

10.2.1   Hall probe Theory

The theory behind hall probes is relatively simple. If we pass current through a conductor, and then apply a magnetic field, then a voltage will be developed perpendicular to the direction of current flow which is proportional to the strength of the applied field.

---

[30]   http://srdata.nist.gov/its90/main/
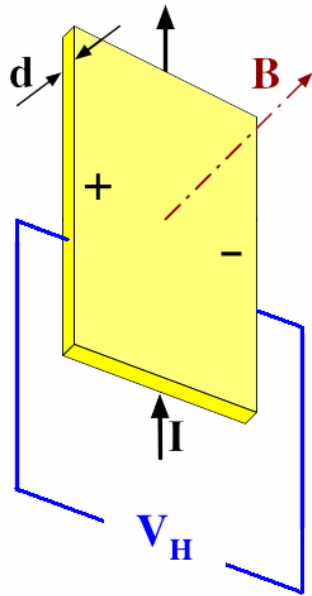
Figure 10-4 – Hall Probe

 The relationship is:

$$V_H = \frac{BI}{ned}$$

Where *B* is the applied field, *I* the current flowing in the probe, n is the bulk carrier density, and *e* the electronic charge.

10.2.2 Testing the hall probes

The probes were arranged as shown below:
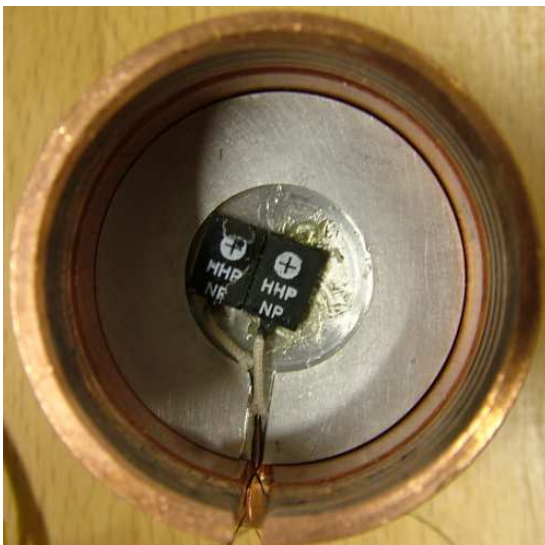
Figure 10-5 – Hall probes mounted inside rig

The two probes are secured to the aluminium washer using melted bees-wax, enabling easy removal. The arrangement of the probes put one sensor (marked by the cross on the sensors surface) closer to the centre of the rig than the other. Any travelling magnetic wave we might observe would be symmetrical, and would reach one before the other, a result we could then observe.

The hall probes could only be tested at room temperature. This was accomplished simply by placing the probe in a magnetic field and comparing its output to that from a calibrated gauss-meter. The manufacturer had provided us with calibration data for room temperature use which proved accurate. We were unable to test the probes at lower temperatures. As the hall voltage depends on carrier density, it will be some function of temperature. However, from discussions with the manufacturer any deviations were expected to be small. A further test could be made by cooling the system in the presence of a known, constant magnetic field and noting how the output changed as the temperature fell.

11 Experimental results

Having successfully tested our sensors, we were in a position to attempt to acquire some results. The first observation was that the change in temperature at our two thermocouples with time was relatively linear, backing up our earlier assumption that the majority of heat transfer was via conduction, and thus validating our thermal model, which neglected radiation.
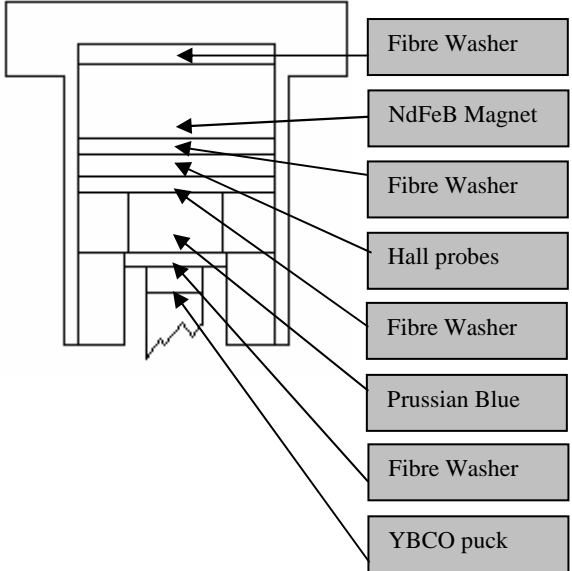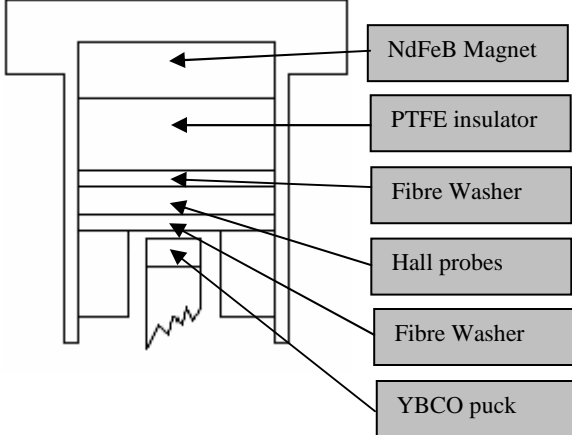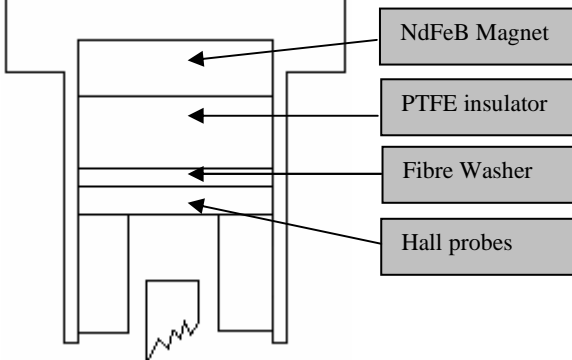
Our first sets of experiments were conducted under the following conditions:

1. Entire Rig (Magnet + Prussian Blue + superconductor)
2. Magnet + superconductor only
3. Magnet only

In each case we used our heater on the top of the rig to apply heat pulses to the system of varying lengths, and observed the results.

11.1 Experimental Geometry

Setup	Geometry	Diagram (not to scale)
1 Fibre washer Magnet Fibre washer Hall probes Fibre washer Prussian Blue Fibre washer Superconductor	Fibre washer thickness: 0.8mm Magnet thickness: 10mm Fibre washer thickness: 0.8mm Hall probe mount thickness: 3mm – probes 2mm above Prussian blue* Fibre washer thickness: 0.8mm Prussian Blue thickness:5mm Fibre washer thickness: 0.8mm Superconductor thickness: 5mm Thermocouples mounted on cold head and level with Prussian blue, on outer surface of copper *It was necessary to mount the probes above the Prussian Blue in this case due to the way in which the Prussian blue puck is held in place from below. A redesign will be needed to bring the probes closer to the YBCO if so desired.*	Fibre Washer NdFeB Magnet Fibre Washer Hall probes Fibre Washer Prussian Blue Fibre Washer YBCO puck
2 PTFE insulator Magnet Fibre washer Hall probes Fibre Washer Superconductor	PTFE washer thickness: 10mm Magnet thickness: 10mm Fibre washer thickness:0.8mm Hall probe mount thickness: 3mm – probes 2mm below Magnet Fibre washer thickness:0.8mm Superconductor thickness: 5mm Thermocouples mounted on cold head and level with magnet, on outer surface of copper	NdFeB Magnet PTFE insulator Fibre Washer Hall probes Fibre Washer YBCO puck
3 PTFE insulator Magnet Fibre washer Hall probes	PTFE washer thickness: 10mm Magnet thickness: 10mm Fibre washer thickness:0.8mm Hall probe mount thickness: 3mm – probes 2mm below Magnet Thermocouples mounted on cold head and level with magnet , on outer surface of copper0mm below top of copper cylinder	NdFeB Magnet PTFE insulator Fibre Washer Hall probes

In each of the three cases care was taken to ensure results were as comparable as possible, by the use of a non magnetic PTFE spacer to take the place of absent parts of the experiment.

11.2 Summary of results

There were three cases examined above:

1 Entire Rig (Magnet + Prussian Blue + superconductor)
2 Magnet + superconductor only
3 Magnet only

Of these, setups 3 and four gave identical results, suggesting that the superconductor was not being magnetized. With the Prussian blue in place however, we obtained very different results, seeming to suggest a magnetization of the superconductor. The only change would appear to be the presence of our Prussian blue material, and some of the data obtained would seem to suggest that our TAS theory was correct. More analysis is needed, however that completed so far is outlined in more detail below.

11.2.1 Magnet only

As the temperature fell, there was a very definite and repeatable signal from our hall probes. The measured field first increased, then fell back to its original value and stabilized there.
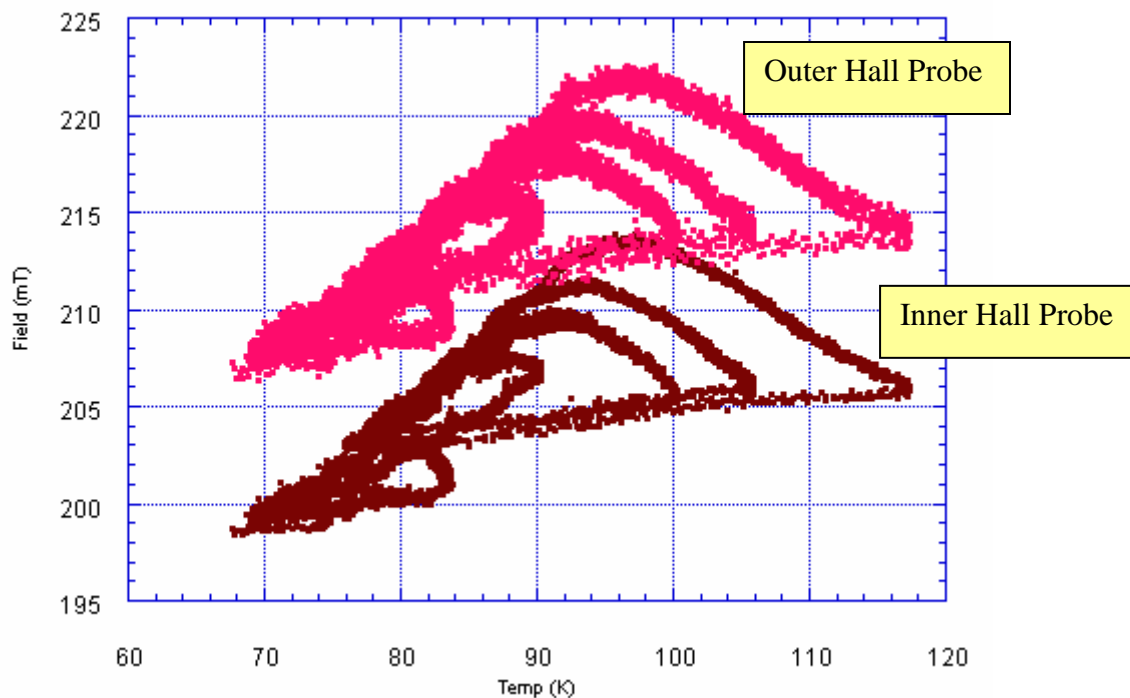
Figure 11-1 – Changes in remnant field with temperature of our NdFeB magnet. Pink (top) plot shows outer hall probe, brown (bottom) shows inner hall probe data.

As would be expected, the hall sensor nearest to the edge of the magnet recorded the highest value, while that closer to the centre recorded a lower value (due to increased flux density at the corners of the magnet). The significant change in remnant field with temperature was unexpected however.

After some research, it was found that this was in fact a characteristic of the NdBFe magnet we were using:
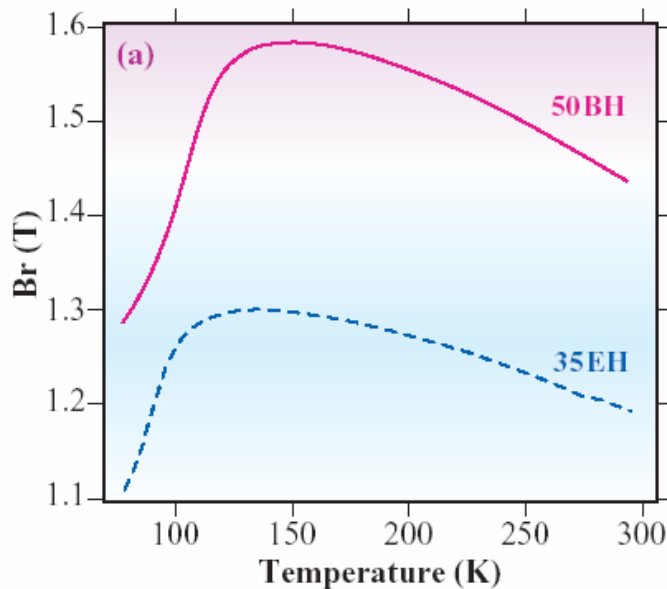
Figure 11-2 – Change in remnant field vs. Temp for NdFeB magnets. Note the magnitudes are different from our own because of the grades of magnet in use.

The above figure shows the dependence of the remnant field to changing temperature. Although not directly comparable to our data (due to a difference in magnet grades between ours and those plotted) the grade affects only the magnitude, not the shape of the data.

While unexpected, it was realised that this variation with temperature could be used to our advantage. The change in remnant magnetic field continues around the ~80K at which our YBCO becomes superconducting. In this case it might be possible, even in the absence of our Prussian Blue, to create a travelling magnetic wave across the surface of the YBCO. If we heat our magnet directly, in place of the Prussian Blue, then as the heat pulse moves inwards so the remnant field changes, and again we have our travelling magnetic wave.

By using our heater, we were able to observe the remnant field of the magnet as we first heated, and then cooled it to different extents – the hysteresis loops thus produced can be seen on the previous page. These loops run clockwise, and appear entirely reversible:
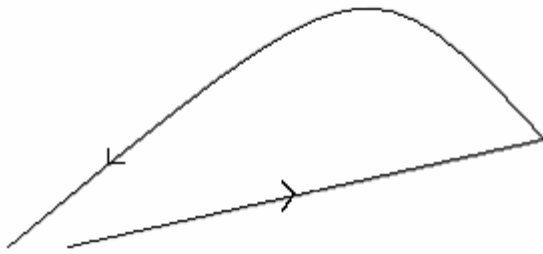
Figure 11-3 - Direction of hysteresis loop

11.2.2 Magnet + superconductor only

The same loops as before were now repeated with the superconductor in place. As before, hysteresis loops were observed – in fact the observed data appears very similar to that observed with just the magnet. In this case there appear to be no observable effects due to the superconductor at all.
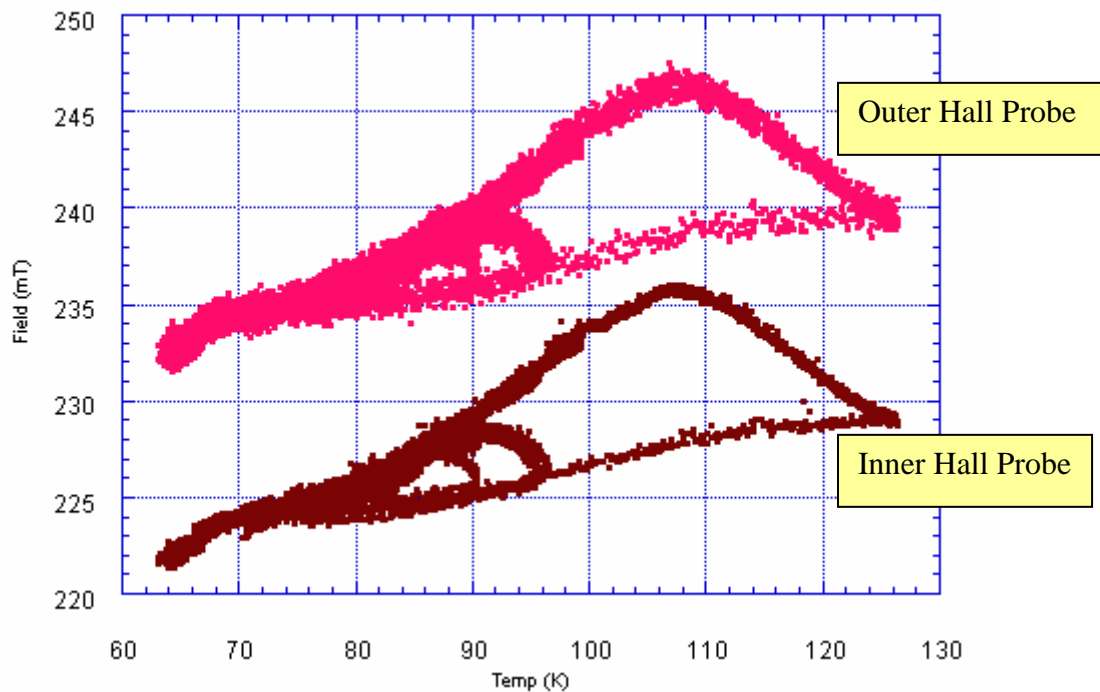
Figure 11-4 - Magnet + superconductor

11.2.3   Comparing Datasets

It was noted that the results obtained with just the magnet, and those obtained with both the magnet and the superconductor appeared extremely similar. An analysis was carried out to determine how similar they were. This was done by closely observing the data recorded over a single heat pulse. Two similar heat pulses were found in both data sets and overlaid:
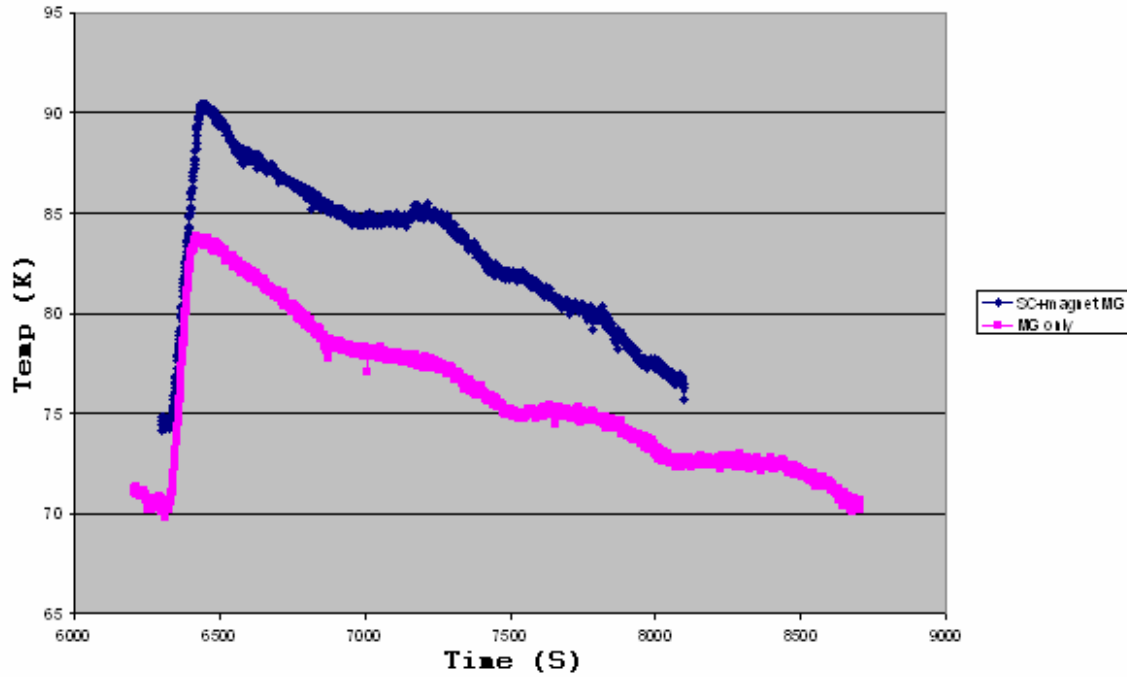
Figure 11-5 – Comparing datasets

The change in measured field over that temperature range for both data sets was then plotted:
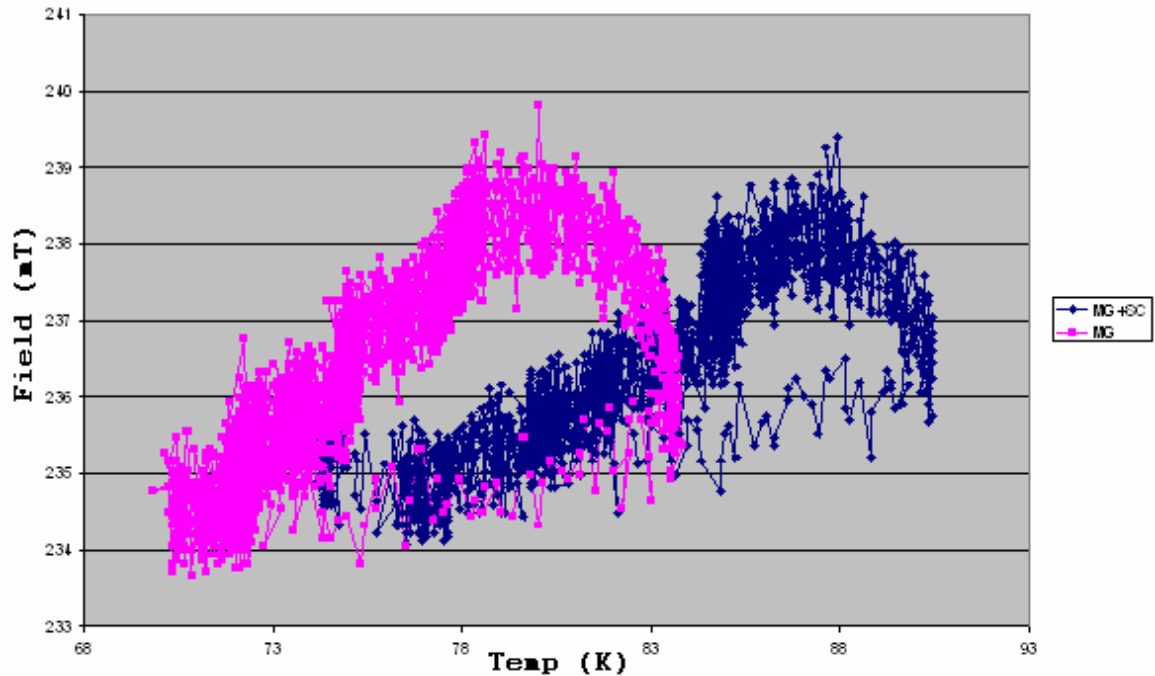
Figure 11-6 – Comparing hysteresis with and without superconductor

It can be seen that the two plots are indeed very similar shape for an identical heat input, although the temperature response of the superconductor sample has been shifted slightly to the right. The loop with the superconductor present also gave consistently higher readings – in the above plot the "magnet only" data has been scaled by 1.12 to make comparison of shapes easier. Whether this change is due to our hall probes or to some effect of the superconductor is unknown at this stage.

11.2.4 Entire Rig (Magnet + Prussian Blue + superconductor)

Finally the same set of experiments were repeated with the entire rig in place – magnet, Prussian Blue puck, and superconductor. To maintain consistency with the earlier setups the hall probes were mounted between the superconductor and the Prussian blue puck. This was not an ideal position, introducing a 3mm gap between the bottom of the Prussian Blue and the top of the YBCO sample. The results obtained are shown below:
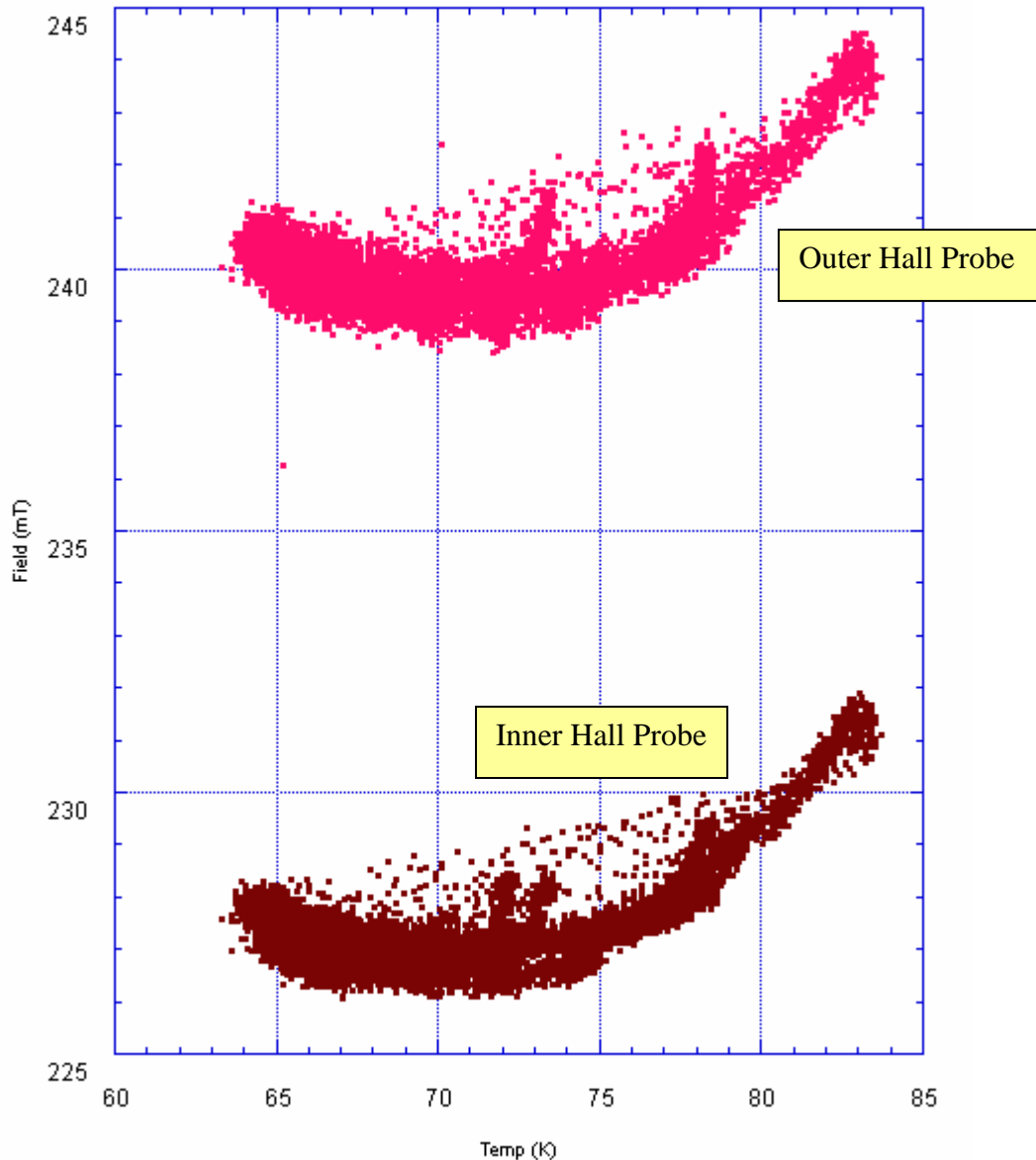
Figure 11-7 – Field vs. temperature for the fully assembled rig

It can be seen that this time there was a very definite effect – our hysteresis loops have been inverted (see Figure 11-3, page76). Previously we heated the system, and then the field increased as it cooled back down again. Now the opposite occurs - while the field still increases linearly with temperature, it then reduces as the system cooled - the fall in field was concave (compared to convex in the previous datasets). This would certainly seem to suggest the YBCO is having some effect on the field – to work out precisely what was occurring more tests were needed.

To check whether we were magnetizing our superconductor, we conducted a series of tests where a heat pulse was first applied to the system, then the change in measured field observed. Plots from this are shown below:
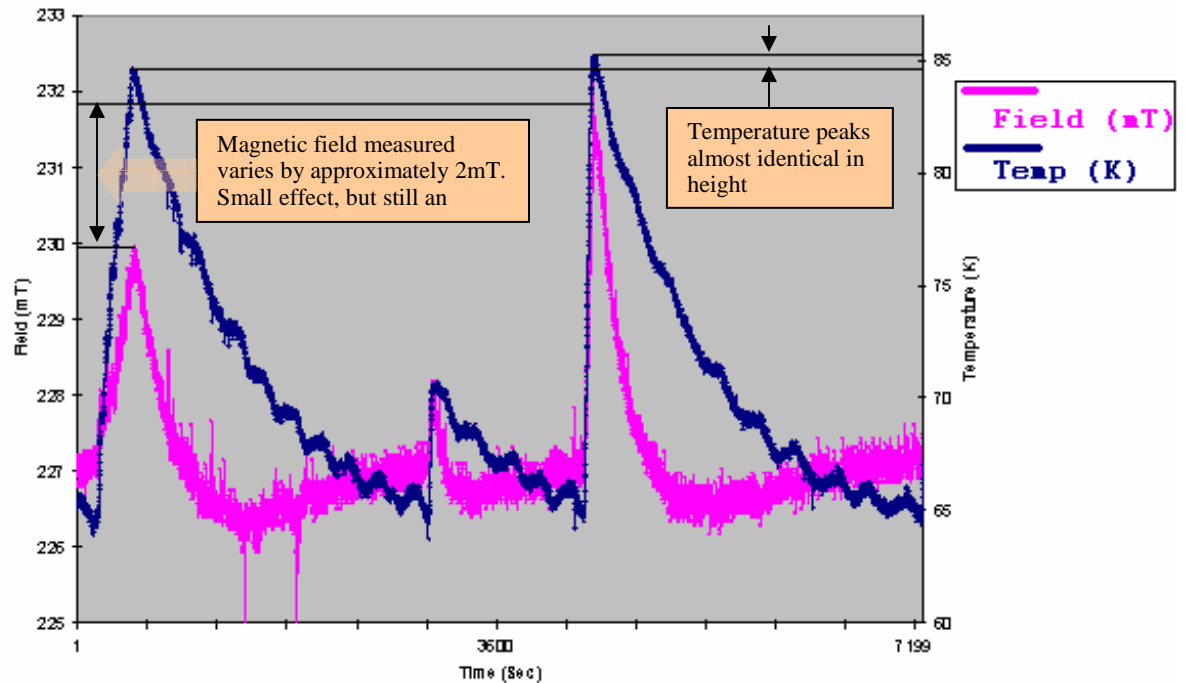
Figure 11-8 - This plot shows the temperature measured at the outer edge of our Prussian blue plotted against the measured field between the Prussian Blue and the YBCO superconductor

This plot would appear to back up our suspicion that we have succeeded in magnetizing our superconductor. It can be seen that we have two temperature peaks of (almost) equal amplitude. The first exhibits a gradual rise in temperature, while the second a far sharper rise.

However, although the magnitudes of the two peaks are almost the same, the magnitudes of the measured field peaks are very different. That produced by the gradually increasing temperature rise has a significantly lower field peak than that produced by the rapid change in temperature.

Had both peaks been the same, the inevitable conclusion would have been that we were merely observing the temperature response of our NdFeB magnet. Since they are not, we need another explanation. Let us start with the assumption that both temperature peaks caused magnetization of our superconductor. Over time, flux creep[31] will cause losses, and so the induced field will reduce.

---

[31] "Theory of Flux Creep in Hard Superconductors" – 12/9/1962 – Physical Review

If the temperature rise is much faster than the losses due to flux creep, then we see a large peak. However, if the temperature rise is slower then the losses due to flux creep are more significant, and the maximum level reached is lower.

The fact that we have observed such noticeable effects attributable to the superconductor in this case, while with just the magnet and the superconductor no such effects were observed would at first appear hard to explain. However, one possible solution is as follows:

The magnitude of the variation in the field of the magnet due to temperature is approximately 15mT. In the case where no effect was observed, the magnet, hall probes, and YBCO were all in close contact. The thickness of the probe mount was 3mm, so the distance between the magnet and YBCO is thus also 3mm.

However, in the second case we have the magnet, then a layer of Prussian Blue analogue, then our probes, and finally the YBCO. As we drive the Blue across its transition, we are inserting a high permeability path between the YBCO and the magnet – effectively bringing the magnet closer. It may be the case that the change in field due to this effect is greater than the 15mT due merely to the temperature dependence of our magnet, and hence the superconductor is affected to a greater extent.

To check this theory we would need to repeat the experiment with just the magnet and the Prussian Blue in place, and then compare the observed change in field at the position of the YBCO with that observed in the same position with only the magnet. Unfortunately time constraints make this impossible to investigate in the context of this MPhil, but it is sure to be thoroughly investigated over the next 12 months by my successors.

Two other phenomena are visible from the above plot. Firstly, there is a ripple with a period of approximately 10 minutes superimposed upon the temperature waveform.
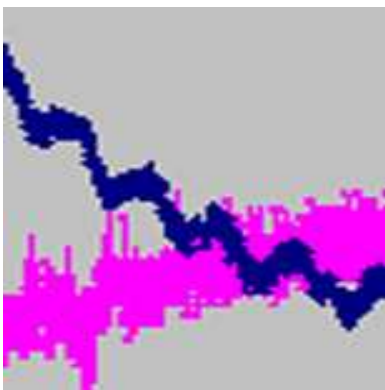
*Figure 11-9- Close-up of the ripple observed in the thermocouples*

 This ripple effect appears to be triggered by the heat pulse, and to die out as the system cools back down after the pulse has been applied. It was initially thought that this could be due to the temperature controller attempting to maintain coldhead temperature, however, even with the controller disabled, the ripple effect continued.

It was then investigated whether the ripple effect could be due to the frequency at which the valves within the coldhead opened and closed, but this was shown not to be the case. It would appear therefore that some kind of thermal resonance is being set up between the cold-head and the top section of the rig. However, it was noticed that the ripple appeared on both the temperature plots for the coldhead itself, and for the copper rig, and was of the same amplitude and phase. However, it did not appear in the hall probe output. Because of the separation of the two points, and the thermal lag introduced by the copper, and the fact that the hall probe values stayed constant it was unlikely that we were observing a true thermal event. This was backed up by the fact that the ripple was only observed when the superconductor was present – while this would not affect the thermal circuit, it will affect the magnetic system. It seems likely then that these oscillations are a result of interference on the thermocouples, perhaps by a changing magnetic field. To test this, a silicone diode has been added to the rig, whose voltage drop is temperature dependant. By passing a known current through the diode and measuring the voltage, we can find the temperature. Furthermore, by first obtaining a baseline by measuring the voltage with no current, we can cancel out any interference not due to temperature effects. This system has been put in place, the circuitry to run the diode built, and the software to interpret the voltages written. However, there has been insufficient time to date to use the diode to test the cause of the ripple.

The second notable feature is the rise in the hall probe output while the temperature is still falling.
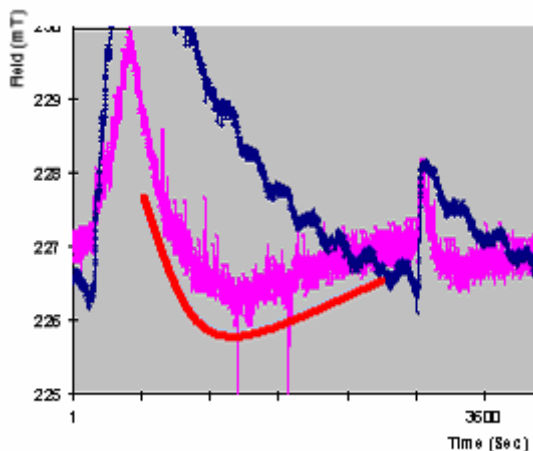
Figure 11-10 – Close-up of the previous plot, showing the magnetic field (pink) rising back, while the temperature (blue) continues to fall

This seems likely to be attributable to the changes in the magnetic properties of the Prussian blue as the system cools. If we had just the magnet in place, the rebound would not appear. However, with the Prussian blue in place, as the temperature falls across the transition temperature, so the relative permeability of the Prussian Blue rises, giving us the rebound effect. More tests are needed at various temperatures and with various configurations to confirm this, but it would suggest that out material is behaving as hoped in concentrating flux as it passes through its ferromagnetic transition.

11.3 Running the system
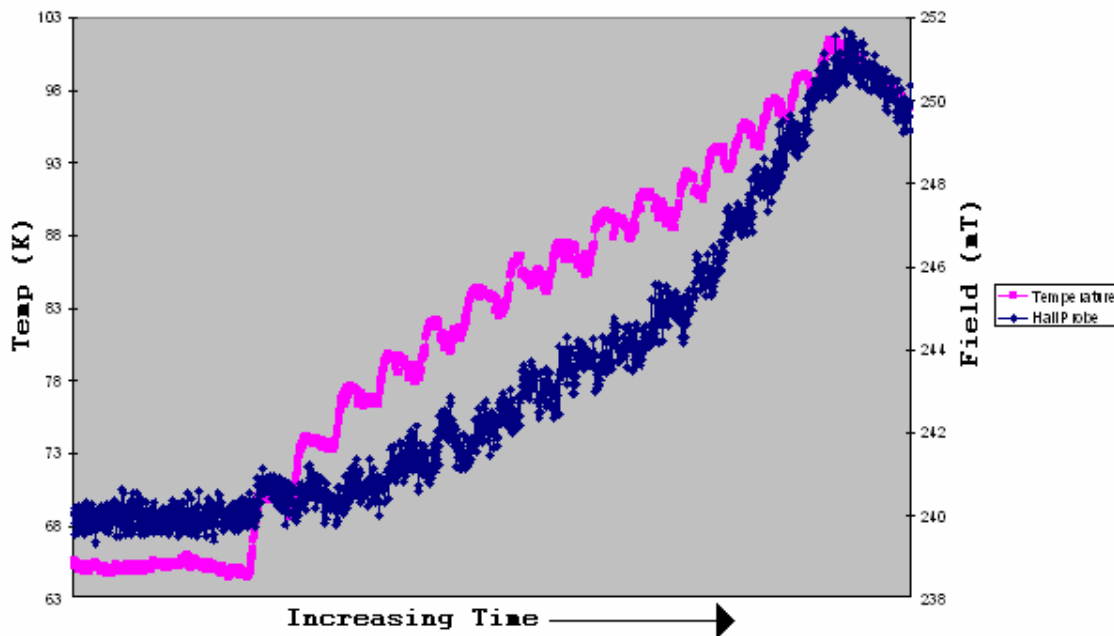
Figure 11-11 – Ratcheting temperature and observing field response

As a final test it was decided to attempt to run the TAS. A series of heat pulses were applied one after the other, as shown above, and the resultant field observed.

It can be seen that while the increase in temperature is linear with respect to time, the increase in measured field is not – the gradient of the field plot is increasing with time. If we are indeed succeeding in producing a TAS, this would be expected (see Figure 4-2, page 21).After each pump we create a stronger field in the same sense as our applied field, and thus when we pump again the field is stronger, and so the next pump has a greater effect. The above plot would appear to suggest this trend.

However it was necessary to check that the observed non-linearity was not merely due to the change in remnant field of the NdFeB magnet with temperature. The temperature range over which the Prussian Blue exhibits its change in properties is unfortunately the same range over which the permanent magnet's remnant field changes significantly.

However, if we compare the above with our plot for the magnet alone (see *Figure 11-1*, page 74) , we see that the change in remnant field over this temperature range is completely linear during heating, whereas what we have observed above is not - suggesting that the above can not be solely due to the changing properties of the magnet with temperature, and giving weight to the proposition that it is, in fact, a result of our TAS concentrating flux as planned. This comparison is not entirely valid as the position

of the hall sensors varied slightly between the two setups (they were closer to the magnet in the "magnet only" readings), however while this might effect the magnitude of the readings, it would not change the shape, and so we are justified in comparing the slopes of the two plots.

However, in any future redesign of the system it would be worthwhile looking at using a solenoid, whose field will not be temperature dependant, to simplify analysis (or making use of a Prussian Blue analogue with a transition temperature a long way from the range in which the magnet changes its field)

12 Future work

As mentioned above, there is clearly still much work to be done in this research field – and to attempt to finish a thesis at such a crucial stage is difficult indeed. There are a (large) number of things that need to be examined over the coming months – more readings to be taken (see above) and possible redesigns to be considered.

It is also worth looking at modifying the rig to address the balance between thermal and magnetic properties. An iron rig has been designed (although not yet built) which should give a far improved magnetic circuit – although the thermal properties may suffer. A further analysis of the conductivity and specific heat of the Prussian blue analogues also needs to be carried out to improve our modelling - this is a task that could be best accomplished via cooperation with colleagues in the Chemistry department.

12.1 Improving Performance

The cryocooler is rated to 10K, however in fact it was only able to achieve a lower limit of ~55K. While this should be low enough to observe the start of any ferromagnetic transition, lower temperatures would enable further study (the temperature transition being from ~65 to ~30K). If in the future other analogues were examined with lower transition temperatures, the need for improving the cooling of the system becomes all the more critical.

The two options for increasing the minimum temperature obtainable were to increase helium flow rate, and to decrease losses from the system. Losses can be reduced by improving the vacuum in the sample space (and thus reducing conduction path), and by reducing radiation from the sample space to the outside world. The vacuum obtainable is already very high (~10^{-7} mbar). However, radiation losses may be reduced by use of a radiation shield (which should cut down radiation by 50% for every layer of the shield). The only disadvantage to this is the very limited space within the sample chamber, and the balance that exists between shielding and experiment.

The only other option for increasing cooling was to increase the helium flow rate to match that of the original compressor (replaced due to old age). This could be achieved to

a limited extent by increasing the voltage supply to the compressor unit, but this will cause it to overheat without an increased chilled water supply.

A final improvement that is needed relates to the temperature control of the coldhead. The current system is standalone, and has limited functionality. A replacement has been designed that will be software based, enabling us to bring the logging of data and the control of the coldhead together on the PC, as well as logging the coldhead temperature. The new system is based around a PIC microcontroller, a solid state relay, and a silicon diode. The diode measures the temperature, the relay switches the coldhead heater in response to the temperature read from the diode, and the PIC communicates with the PC over RS232. The schematics for this system have been drawn up, but the system itself is not complete – the interface software for the PC is still to be written, although it is not expected to present a problem – a simple VB application is expected to suffice.

13 Temperature controller schematic

Figure 13-1 – Schematic of temperature controller design

14 References

Title	Journal	Issue	Date	Author(s)
Ion-exchange synthesis and magneto-optical spectra of colored magnetic thin films composed of metal(II) hexacyanochromates (III)	ChemComm	Issue 10, Pages 1204-5	May 2003	M. Tozawa ,S. Ohkoshi,N. Kojima,K. Hashimoto
New Magnetic Functionalities presented by Prussian Blue analogues	Electrochemical society Interface	Vol. 11, No. 3 - p. 34	Fall 2002	Shin-ichi Ohkoshi and Kazuhito Hashimoto
Electrons at work in Prussian Blue Analogues	Electrochemical society interface	Vol. 11, No. 3 p. 28	Fall 2002	M. Verdaguer, N. Galvez, R. Garde, and C. Desplanches
Is it possible to Get High TC Magnets with Prussian Blue Analogues? A Theoretical Prospect	Chemistry - A European Journal	Volume 11, Issue 7 , Pages 2135 - 2144	March 18th 2005	Eliseo Ruiz, Dr. 1, Antonio Rodríguez-Fortea, Dr. 1, Santiago Alvarez, Prof. Dr. 1, Michel Verdaguer, Prof. Dr.
A Prussian Blue Type Ferrimagnet Na[MnCr(CN)$_6$]: Single crystal structure and magnetic properties	Inorganic Chemistry	Volume 8, Issue 42 2004 Pages 2465-2467	April 19th 2004	Dong W,Zhu LN,Song HB,Liao DZ,Jiang ZH,Yan SP,Cheng P,Gao S
Demagnetization factors for the general ellipsoid	Physical Review	Phys. Rev. 67,351 - 357 [Issue 11-12]	24 March 1945	J. A. Osborn
Theory of Flux Creep in Hard Superconductors	Physical Review Letters	Issue 7, pages 309-311	12 September 1962	P. W. Anderson

Papers

Patents

Patent number	Title	Patent Office	Author
GBP290529	Superconducting Systems	UK Patent Office	Dr. Tim Coombs
239481	Pyromagneto-electric generator	US patent office	Nikola Tesla

Books

Title	Author	Publisher
Matter and Methods at Low Temperature	Frank Pobell	Springer, 2002
Ferromagnetism	Richard M Bozorth	D. Van Nostrand, 1951